BACHELOR THESIS

BIOMEDICAL ENGINEERING

Universidad
Carlos III de Madrid

STUDY OF THE RESONANT BEHAVIOUR OF BUBBLES EMBBEDED IN GELATIN

AUTHOR

Judith Cueto Fernández

TUTORS

Patricia Vega Martínez

Miguel Parrales Borrero

Javier Rodríguez Rodríguez

Department of Thermal and Fluids Engineering

Science is not only a discipline of reason but, also, one of romance and passion.

- Stephen Hawking

Table of contents

List of figures

Acronyms

ABS - Acrylonitrile butadiene styrene

CEUS - Contrast-specific ultrasound

ePHD - Extended pure harmonic detection

LDPE - Low-density Polyethylene

mPAP - Mean pulmonary artery pressure

PAH - Pulmonary arterial hypertension

PFC - Perfluorocarbons

PLGA - Poly-(D,L-lactideco-glycolide)

SF_6 - Sulfur hexafluoride

SHAPE - Sub-harmonic aided pressure estimation

SNR - Signal-to-noise ratio

UCA's - Ultrasound contrast agents

US - Ultrasounds

Abstract

Many diseases present abnormally high pressures at different points of the circulatory system, such as inside the heart, the portal vein or the pulmonary artery. For this reason, physicians need to know the pressure at these specific points either to help diagnosis or to monitor the evolution of a patient's condition. Nowadays, these pressure measurements are performed invasively, for instance by navigating a catheter with a pressure sensor at its tip to the point of interest. As any invasive procedure, acquiring these measurements presents a number of shortcomings that medical doctors would like to avoid. Consequently, providing physicians with a non-invasive pressure measurement technique would represent a great advance in the diagnosis and/or treatment of these patients.

Ultrasound Contrast Agents (UCAs), microbubbles injected into the blood stream to aid ultrasonic imaging, offer the possibility of obtaining the blood pressure at localized points of the circulatory system in non-invasive ways. Indeed, it can be shown mathematically how these microbubbles oscillate at a characteristic frequency (resonance frequency) when insonated with a pressure pulse with the appropriate features. More interestingly, it can also be shown that this resonant frequency depends on the ambient pressure at the bubble's location.

With these ideas in mind, in this thesis we have conducted an experimental and numerical investigation aimed at measuring how the resonance frequency of bubbles immersed in gelatin depends on the ambient pressure. Since the focus of this work is on the Physics, rather than on implementing a practical technique, we have worked with millimetric bubbles (commercial UCAs are micrometric) in order to overcome a number of experimental problems associated with using very small bubbles. Furthermore, fixing the bubbles in gelatin also allows for a prolonged observation and thus facilitates the experiments. But at the same time, gelatin constitutes a very realistic model of the rheological properties of the soft tissue that would surround bubbles in some real medical applications (think, for instance, of a bubble circulating through a narrow capillary surrounded by soft tissue).

In our experiments, bubbles are insonated with chirps: pressure pulses that sweep a range of frequencies that contains the resonance one. Then, the radius vs. time evolution of the bubbles is obtained by applying digital image processing techniques to high-speed movies acquired synchronously with the acoustic insonation. Finally, the time evolutions of the bubble radii are processed using wavelets to extract the main frequency at which they oscillate.

Although the experimental procedure designed and implemented in this thesis detects that bubbles oscillate at a well-defined frequency close to the expected resonance ones, our numerical simulations and the analysis of the pressure signals reveal that this frequency is actually arising from an improper behavior of the piezoelectric transducer used to generate the pulses.

Finally, we point out future lines in which this work could be improved, most notably replacing the transducer by another one that performs better in the range of frequencies of interest. This solution is being implemented at the time of writing this dissertation.

1. Introduction

1.1. Motivation

Ultrasound contrast agents

The use of ultrasound (US) as a diagnostic tool has been a common approach in medical imaging since the 1960s due to the possibility of obtaining real-time images, its low cost and the lack of ionizing radiation. The principle behind it consists in the differences in acoustic impedance that body tissues exhibit. Ultrasonic waves (20 kHz or higher) are sent through tissues using a piezoelectric transducer (a device that transforms electrical energy into mechanical energy, and vice versa) and the backscattered intensity is measured by a receptor, which in most cases is the same transducer. The intensity of the scattered sound is proportional to the impedance mismatch between tissues, and thus allows for their differentiation and the creation of an image. Nevertheless, the quality of these images by themselves is not always high enough for a proper diagnosis, and this need for enhancement lead to the discovery of ultrasound contrast agents (UCA's).

The application of UCA's to enhance blood pool contrast was firstly reported in 1968 by Gramiak and co-workers [1] when an increase in the echo backscattering in the aorta after injection of a saline solution was observed. It was later discovered that this enhancement in the received signal was caused during catheterization by the formation of air microbubbles through cavitation [2, 3]. The reason why the presence of these microbubbles yields better resolution images is that the impedance difference between the bubbles and blood or surrounding tissue is very large. This causes a high backscattering of the incident wave by the bubbles, producing a greater contrast in the resulting images (Fig. 1). Nevertheless, it wasn't until the 1980s that scientists overcame the obstacle of these bubbles quickly dissolving into the blood stream. In order to increase bubble stability and durability in peripheral circulation, two approaches were developed: the external encapsulation of microbubbles, adding a surfactant in some cases, and the replacement of air with less soluble gases with low diffusion coefficient. The microbubbles were coated with lipids [4] (Fig. 2), proteins [5] or other biopolymers [6], and some of the used gases that have yielded the best results are perfluorocarbons (PFC) and sulfur hexafluoride (SF_6) [7]. These modifications allow for the contrast agents to keep into circulation for larger time periods, increasing the quality of diagnosis.

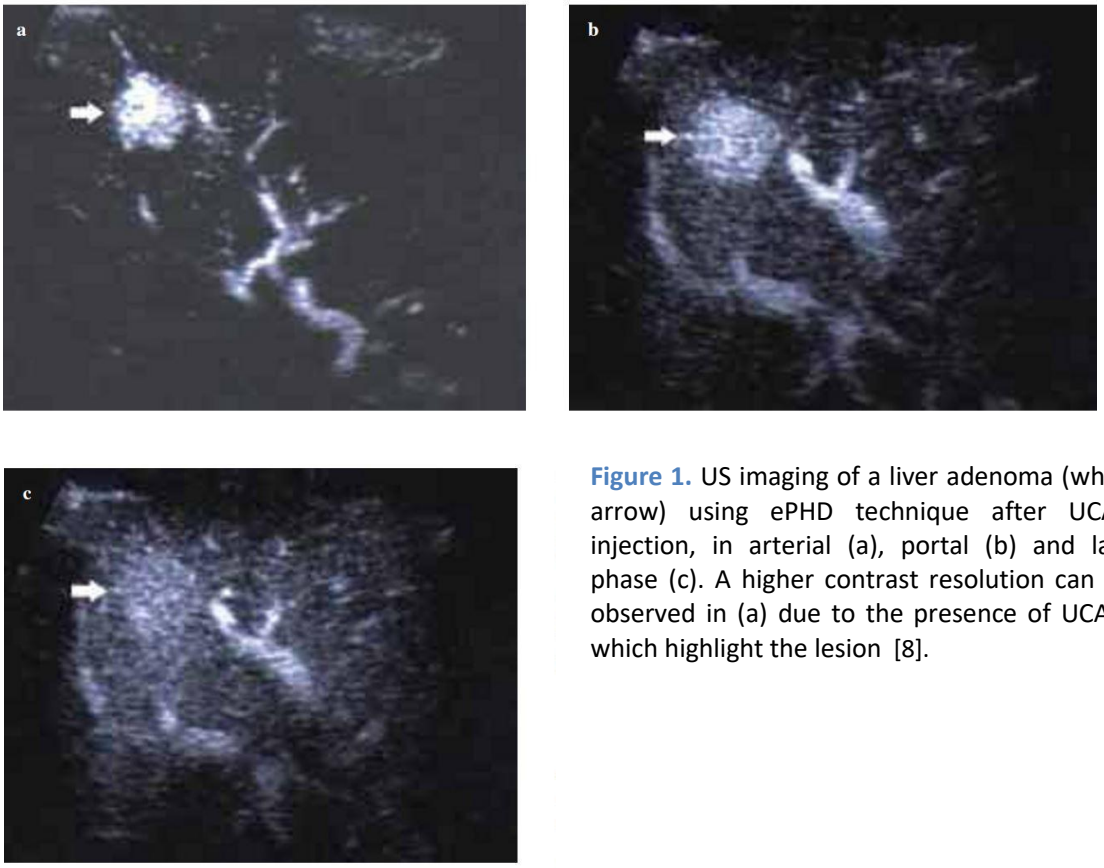

Figure 1. US imaging of a liver adenoma (white arrow) using ePHD technique after UCA's injection, in arterial (a), portal (b) and late phase (c). A higher contrast resolution can be observed in (a) due to the presence of UCA's, which highlight the lesion [8].

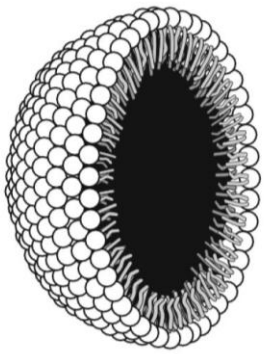

Figure 2. Schematic representation of a phospholipid-coated microbubble [9].

By definition, UCA's are colloids, formed by a dispersed phase (microbubbles) distributed uniformly in a dispersion medium (blood). Current UCA's are intravenously administered microbubbles composed of a biocompatible shell and a high-molecular-weight low-solubility filling gas. Their diameter ranges from 3 to 10 µm [10], as it needs to be small enough to pass through pulmonary circulation in order to be used in the visualization of the left side of the heart. In Fig. 3 a comparison between commercial UCA's and red blood cells is depicted, showing their diameter is smaller than that of the cells, which prevents them from being filtered by the lungs and thus allowing them to continue into the circulation.

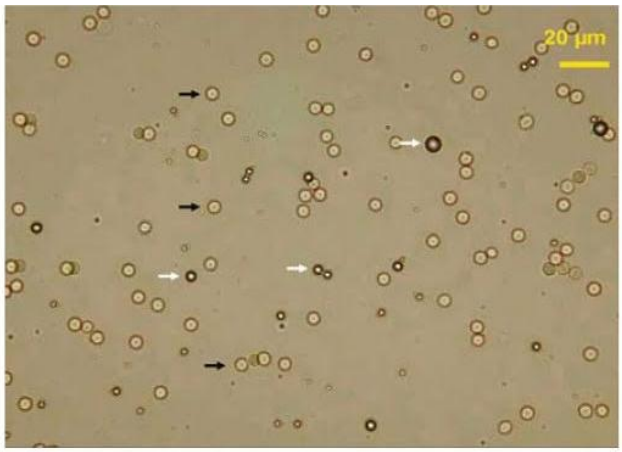

Figure 3. Two-dimensional microscopic snapshot of commercial UCA's SonoVue (white arrows) in comparison with red blood cells (black arrows) [11].

The role of the microbubble shell is to avoid the problems of gas diffusion and bubble coalescence (the process by which two bubbles merge, generating a larger one), with the consequent breakup. The shell prevents the gas volume inside the bubble from changing dramatically as a consequence of the difference in gas concentration with the blood. This coating also increases the energy threshold that two bubbles need to overcome before merging, causing this way a repulsive force between them if they approach too much [12]. This translates into a better imaging performance and higher safety for the patient, as the presence of larger bubbles in the bloodstream, generated by coalescence, entails the risk of gas embolism [13, 14]. The shell composition can be tuned depending on the application, making it flexible or stiff, and presents a thickness ranging from 100 to 200 nm [11]. Some examples of the biocompatible molecules constituting the shell of commercial UCA's are: galactose/palmitic acid in the case of Levovist (Schering), albumin in Optison (GE Healthcare), poly-(D,L-lactideco-glycolide) (PLGA) in AI-700 (Acusphere), and Phosphatidylserine in Sonazoid (GE Healthcare). These and other readily available commercial UCA's used in medical ultrasound are listed in Table 1.

The perfect UCA should be filled with a gas that hardly diffuses through its shell and that is not soluble in blood. Currently, the best approximation to this ideal model has been the replacement of air with perfluorocarbons and sulfur hexafluoride. These gases hardly diffuse through the phospholipid coating.

Name	Shell composition	Gas	Manufacturer
AI-700	Polymer	Perfluorocarbon	Acusphere
biSphere	Gelatin/polymer	Air	Point Biomedical
BR14	Phospholipid	Perfluorobutane	Bracco Diagnostics
BY 963	Lipid	Air	Byk-Gulden
Levovist	Galactose/palmitic acid	Air	Schering
Definity	Lipid	Perfluoropropane	Bristol-Myers Squibb
Imagent	Surfactant	Perfluorocarbon	Imcor Pharmaceuticals
Optison	Albumin	Perfluoropropane	GE Healthcare
Sonazoid	Lipid	Perfluorobutane	GE Healthcare
SonoVue	Surfactant	SF6	Bracco Diagnostics
MRX-408	Lipid/ligand oligopeptide	Perfluoropropane	ImaRx
Quantison	Albumin	Air	Andaris Ltd
QFX	Albumin	Perfluorocarbon	Guangzhou Nanfang Hospital

Table 1. List of commercial UCA's and their composition [15].

The shell chemical composition and inner gas choice has an effect on the acoustic behaviour of the bubbles, showing differences in their harmonic response[1] [7], together with their fate after being administered *in vivo*. 10 to 15 minutes after being intravenously injected, UCA's are degraded. Their gas content is exhaled via the lungs [16] and their shell is metabolized or filtered by the kidneys and eliminated by the liver [11]. In addition to this, some microbubbles show a post-vascular hepatic or splenic phase before being degraded, caused by the adhesion of the bubbles to the hepatic sinusoids or their selective uptake by the reticuloendothelial system phagocytic cells, which allows for an enhanced visualization of the mentioned organs [17-22].

When being used in humans, UCA's show a very good safety profile and a lack of renal, liver or cerebral toxicity [23]. The rarely observed adverse reactions are usually soft and transitory [23, 24].

Ultrasound techniques and UCA's usual applications in diagnosis

When performing contrast-enhanced medical ultrasonography, contrast agents can be insonated in two ways, which determines their harmonic response. Microbubbles are acoustically excited at their resonance frequency, a concept that will be explained in more detail in subsequent sections, by using a high- or low-transmit power.

In high-transmit-power modality, the acoustic pulse amplitude is of the order of 1MPa and causes the destruction of the microbubbles, producing a wideband harmonic signal that resembles an explosion. It is used with air-filled contrast agents with a soft

[1] Harmonic response refers here to oscillations (periodic compression and expansion of the bubble radius) occurring either at the resonance frequency or at an integer multiple of it.

shell, that would exhibit a mild response in a lower intensity insonation approach. This modality is characterised by the transience of the received signal.

In low transmit power method, the amplitude of the acoustic signal is smaller, ranging from 30 to 70 kPa, and it exploits the nonlinear response of microbubbles when being insonated at their fundamental frequency. The oscillations induced in the bubbles emit a signal containing the fundamental frequency and other subharmonic frequencies (multiples of the fundamental one), which can be exploited to generate an image. This modality is applied together with SF_6- or PFC-filled microbubbles with a strong shell, which allows for real-time prolonged organ visualization.

UCA's have proven to be of great utility when improving blood flow detection and vasculature depiction using Doppler ultrasonography, either color or power Doppler, by increasing the signal-to-noise ratio (SNR). Nevertheless, these techniques have major limitations because of blooming artifacts and signal saturation, which made necessary to develop contrast-specific ultrasound (CEUS) techniques. These allow for the enhancement and visualization, not only of blood pool and vessel patency, but also of perfused tissues and even organs with scarce vasculature, as it is the case of the urinary bladder. Among these different approaches, a broad classification can be established [8]:

- *Pseudo-Doppler techniques*. These methods are based on multipulse high-transmit power insonation, and rely on the detection of the aforementioned wideband signal, characteristic of the high power approach. The techniques this modality comprehends are: stimulated acoustic emission, cadence agent detection imaging, advanced dynamic flow, and tissue signature imaging.

- *Harmonic imaging techniques.* They use multiple pulses and are based on the nonlinear physical behaviour that microbubbles exhibit when insonated at their resonance frequency. Most of them attempt at suppressing the stationary tissue background by detecting the second harmonic (twice the value of the fundamental frequency), which ideally does not contain any component from the tissue response, but only from the bubbles oscillations. Nevertheless, in real applications these techniques are limited due to the presence of harmonics from the surrounding tissue when insonated at high transmit power, which can overlap with the secondary harmonic and diminish the spatial resolution of the images. They can be performed using low or high transmit power insonation. Some of the techniques in this modality are: gray-scale harmonic imaging, extended pure harmonic detection, flash echo imaging, harmonic power-doppler imaging, contrast-tuned imaging, c-cube, ultraharmonic imaging, and subharmonic imaging.

- *Phase modulation techniques.* These techniques lie in the usage of multiple pulses per scan line, using low transmit power. These pulses are inverted replicas of each other, and through the posterior processing of the received signals it is possible to cancel the acoustical components received from surrounding tissues and increase the SNR of the bubbles response. Some of the techniques this approach comprises are: pulse inversion harmonic imaging (with two transmissions), microflow imaging, contrast tissue discriminator, power pulse inversion (with three transmissions), and vascular recognition imaging.

- *Amplitude or power modulation techniques.* These techniques rely on alternating varying-power pulses instead of varying-phase pulses, also using the low transmit power approach. The linear response of stationary tissue accounts for cancellation between the received signals, whereas the echo produced by the nonlinear behaviour of the bubbles enables for the creation of an image.

- *Amplitude and phase modulation technique: Cadence contrast pulse sequencing (CPS).* This technique fuses the two previously described approaches, in order to obtain a better image spatial resolution.

There exists a wide range of clinical applications for UCA's in medical ultrasonography, that have continued to grow throughout the last decades. The organ in which CEUS shows the most reliable results is the liver, exhibiting an accuracy similar to that of computerized tomography (CT) and magnetic resonance (MR) for focal liver lesion characterization [25-28]. It is also useful in the evaluation of the portal vein state in cirrhosis and liver transplantation [29], and for the differentiation between benign and malignant thrombosis in the aforementioned vein [30, 31]. US in combination with UCA's is also employed in the detection of spleen infarctions [32, 33] and in the differentiation between benign and malignant splenic tumors [33]. CEUS is also yielding promising results in monitoring radiofrequency ablation of renal tumors, among others, in animal models [34].

Another widely extended use of CEUS includes echocardiography for the right and left ventricles. It helps in assessing the existence of shunts (holes that allow for the passage of fluid between two body parts), abnormalities on the great vessels, cardiac structure, valvular function and wall motion. Other applications comprehend perfusion quantification and evaluation of myocardium [35, 36]. UCA's mediated US has also been employed in the improvement of tight stenosis quantification of the carotid and peripheral arteries [37], and in the visualization of intracranial arteries [38].

UCA's novel applications in theranostics

As presented in previous sections, the use of UCA's in the enhancement of medical ultrasound images for diagnostic purposes is a usual and widespread approach nowadays, but this is not their only function. Many different applications have shown up over the last decades, which involve their usage both in diagnosis and treatment.

- **Molecular imaging.**

The idea of using UCA's for molecular imaging diverges from the concept of bubbles passively travelling through the bloodstream. For this new approach, site-specific microbubbles are employed, which surface is coated with specific ligands in order to reach the point of interest.

Molecular imaging via US mostly uses intravascularly injected microbubbles that bind to disease specific epitopes on the surface of endothelial cells. This specific adhesion due to the presence of targeting ligands on the surface of UCA's is exploited as an imaging tool, since when being insonated with US, microbubbles exhibit their characteristic nonlinear response that can be detected as a persistent contrast effect on a 2-dimensional US image.

An example of one approach used to target the microbubbles is the attachment of monoclonal antibodies to their shell in order to bind to activated endothelial cells adhesion molecules, as the inflamatory marker P-selectin, and tumoral angiogenic markers as αv-integrin [39]. This, and other targeting techniques allow for the *in vivo* detection via US of phenotypic endothelium features that are linked to clinical diseases, facilitating diagnosis [40, 41]. Moreover, the recently used acoustically active nanoparticle emulsions, capable of entering cells due to their size, may allow for new possibilities for visualization of intracellular processes [42].

- **Acoustic lysis.**

Exploiting the same targeting techniques utilised for UCAs-mediated US molecular imaging, microbubbles can be targeted to specific sites in the vascular system, where a thrombus is present. Taking advantage of their acoustical response, the microbubbles are insonated at high power once they reach the point of interest, causing their explosion by cavitation (Fig. 4), and helping in the dissolution of the thrombus [43]. The same approach can be employed for kidney stone destruction (lithotripsy) and tissue ablation (hytotripsy) [44, 45].

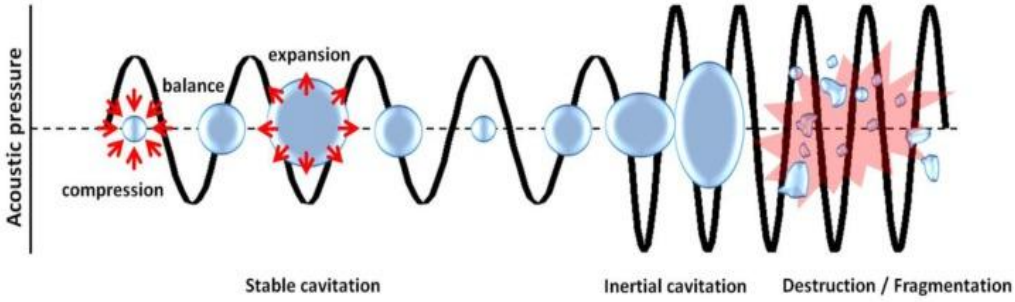

Figure 4. Schematic representation of a bubble exhibiting radial oscillations and eventually undergoing cavitation [46].

- **Drug delivery.**

The idea of using UCA's as drug and gene delivery vectors has also been exploited in the last years. This can be done by targeting the microbubbles to specific cells or by means of US waves, which due to radiation force (Bjerknes force) are capable of displacing the bubbles in the direction of the wave, directing them through the bloodstream and towards the site of interest. Drugs can be attached to the microbubbles surface or be entrapped with the gas in their interior. Once the bubbles are at the desired location, bubble breakup occurs due to high transmit power US, releasing the drug [40, 46-48].

- **Pressure measurement.**

Over the past 30 years scientists have been considering the use of microbubbles in the development of a noninvasive pressure measurement technique. This idea was first proposed in 1977 by Fairbank and Scully [49], who, based on the equations formulated by Minnaert in 1933 [50], observed a frequency shift in the bubbles response (while being insonated at their resonant frequency) at different ambient pressures. This discovery lead scientists to search for a way in which the characterization of this change in the bubble acoustical response could be used in order to determine the pressure around it. Several approaches have been proposed in the literature since this effect was first noticed, which will be discussed in section 1.2 (*Microbubbles-based Noninvasive Pressure Measurement Techniques: State-of-the-art*), although the implementation of any of these techniques into clinical scenarios has not been possible yet. Nevertheless, despite of the differences in these approaches, all of them are based on the same principle: the exploit of the bubble behaviour changes depending on ambient pressure.

This physical behaviour also applies to commercial UCA's, and thus when ultrasound waves are focused on them they oscillate either linear or nonlinearly at their natural frequency, depending on the intensity of the applied field. The final goal of these approaches is to detect the changes in the harmonic response of UCA's intravenously

injected in a patient, and to use this information to determine the pressure at that particular point in the vascular system.

Bubbles as linear oscillators

When a driving force, such as an acoustic wave with wavelength much larger than the bubble diameter, is applied on the medium where a bubble resides, the pressure pulse generated by this wave excites the bubble and makes it oscillate. Under this scenario, the bubble can behave in three different ways depending on the intensity of the driving force [51]: it can expand and compress so quickly that it collapses, it can oscillate nonlinearly, or it can oscillate linearly (in a pulsating way) about its equilibrium radius. The parameter that determines which motion type the bubble will experience is the amplitude of the pressure wave applied on it. Thus, for large amplitudes the bubble will collapse, while reducing the intensity will lead to nonlinear and finally linear oscillations.

In the linear regime, when a pressure wave traverses the medium, the bubble will compress while the pressure is positive, and expand when it is negative (Fig. 5. (a)). This will cause a periodic radius variation of small amplitude during the time the bubble is under the pressure field. Once the driving force is removed, these oscillations will continue until the drag force produced by the pressure differences created upon compression and expansion of the gas inside the bubble overcome the inertial force exerted by the surrounding medium (liquid or gel) on the bubble surface.

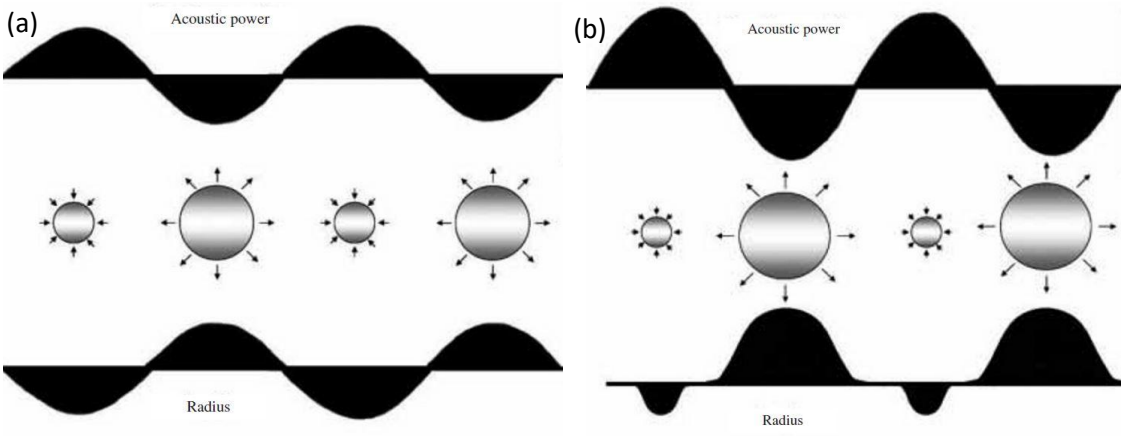

Figure 5. Schematic representation of bubble oscillations in linear and nonlinear regime, depending on the insonating acoustic pressure [8].

The frequency that dominates these oscillations is the natural frequency of the bubble, which is strongly dependent on its size and ambient pressure, as it can be deducted from the equation formulated by Minnaert [50]:

$$\omega_0 = \sqrt{3\gamma P_0/\rho R_0^2}\ ,$$

where P_0 is the pressure at the bubble location, R_0 is the bubble radius at equilibrium, ρ the density of the surrounding medium and γ the polytropic index of the gas. The further development of this formula together with a deeper explanation of its implications to the noninvasive measurement of the ambient pressure will be discussed in the section 2 (*Theoretical Background*).

The difference between these linear oscillations and nonlinear ones resides in the ratio between compression and expansion of the bubble. In the nonlinear regime, bubbles are less resistant to expansion than to compression, which produces asymmetric oscillations, as depicted in Fig. 5. (b). Consequently, a bubble experiencing nonlinear oscillations emits an acoustic response in which there is, not only the fundamental frequency component (resonance frequency of the bubble), but also other harmonic components which are multiples of the fundamental one, both subharmonics (half its value) and ultraharmonics (higher multiples). An example of the difference in the power spectral density[2] of a linear and nonlinear oscillating bubbles is illustrated in Fig. 6.

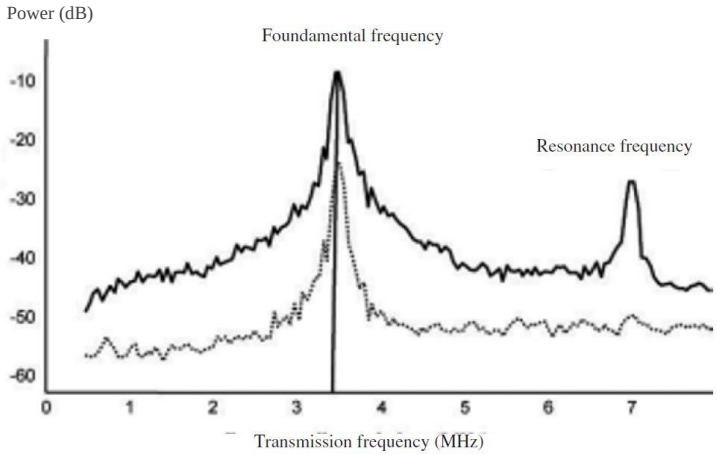

Figure 6. Power spectral density of SF_6-filled microbubbles exhibiting a linear response (dashed line) and nonlinear response (solid line) [52].

Arterial pressure measurement

The measurement of blood pressure in points of difficult access in the vasculature, as the heart cavities or the major vessels (such as the aorta) is an important parameter when assessing patients with valvular heart disease, congestive heart failure, and other vascular diseases. It is also necessary for the diagnosis of pulmonary arterial hypertension (PAH), a disorder characterized by a decrease in the distal pulmonary

[2] In simple terms, the power spectral density refers here to the power that the sound emitted by the bubble has at different frequencies.

arteries blood flow due to a reduction in vascular cross-sectional area, producing right ventricular pressure overload (mean pulmonary artery pressure (mPAP) >25 mmHg instead of the 10-20 mmHg representative of a healthy condition), and ultimately leading to right-heart failure and death if untreated [53, 54]. Currently, there exists no definitive treatment for this condition, although several effective therapies are being developed, based on targeting the specific aberrant pathways that lead to this modification of vascular tissue [55, 56].

The clinical measurement of the mPAP can only be performed with the needed accuracy in an invasive way for the moment, by means of right-sided heart catheterization. This invasive procedure results in an increase in the patient's risk of contracting infections, together with pain and discomfort. For these reasons, a noninvasive approach capable of providing these measurements in an accurate and reliable way would result in a wide range of benefits both for the patient and the physicians. A noninvasive approach that is already being used in clinical diagnosis is based on the detection of the right ventricle wall movement using conventional US imaging by means of Doppler echocardiography. Nevertheless, this estimation of blood pressure is not accurate enough for a proper diagnosis, and it can only be used as an aid to estimate whether it is probable a patient suffers from PAH, and proceed to a right-heart catheterization to verify it [57].

Thus, the development of a noninvasive pressure measurement technique based on the usage of UCA's and ultrasonic waves would be of great help in the diagnosis of this disorder, as it would provide clinicians with accurate measurements in a quick and easy way. Based on this, together with serving physicians as a great diagnostic tool for several types of cardiac diseases as it is the case of PAH, this method would also have applications in intensive care settings, helping for instance in managing medication levels for heart failure patients, showing the greatly wide range of possible uses for this technique.

1.2. Microbubbles-based Noninvasive Pressure Measurement Techniques: State of the art

Since 1977 several groups have proposed different approaches to develop a noninvasive pressure measurement technique based on the behaviour of microbubbles injected in the bloodstream. The main lines of investigation in this topic can be classified as follows.

Study of the amplitude of the subharmonic

As explained before, when an acoustic field with an amplitude of 30-70 kPa is applied to a microbubble, this behaves as a nonlinear oscillator and the power spectral density of its response exhibits the aforementioned harmonics in addition to the fundamental component. In 1999, Shi *et al.* [58] proposed that by measuring the intensity of the subharmonic peak, it was possible to determine the ambient pressure, as it was proven to exhibit a linear variation when plotted against the pressure. This technique was named SHAPE (Sub-Harmonic Aided Pressure Estimation) and allowed them to successfully measure pressures in their laboratory.

More recently, Halldorsdottir *et al.* [59] applied the SHAPE technique to determine the *in vitro* subharmonic response of several contrast microbubbles, setting different ambient pressures and acoustical parameters. In addition to this, in 2011 and 2012, they performed *in vivo* experiments for the assessment of portal hypertension and right ventricular pressure estimation [60-62], although the technique employed has not been implemented into clinical procedures for the moment. They concluded that the subharmonic intensity is a good indicator of the ambient pressure and thus, the SHAPE technique represents a powerful diagnostic tool in clinical scenarios.

In addition to this, Li *et al.* [63] employed a hybrid approach consisting in the detection of the frequency shift experienced by the subharmonic peak with ambient pressure variations. In fact, they were able to measure this shift, although the obtained values were twice as large as the expected ones, showing a discrepancy with the theory.

In 2009, Andersen & Jensen [64] carried out a parametric study to better characterize the changes in the subharmonic peak with the ambient pressure, which again proved the existence of this linear relation between them. One year later, they also performed experiments using Sonovue (Bracco Diagnostics), in which they intended to find how changes in ambient pressure affect the ratio between the energy of the subharmonic and the fundamental components [65]. Nevertheless, as the authors themselves point out in their work, this technique has several weaknesses despite of the impressive results obtained. These shortcomings reside in the fact that the amplitude of the subharmonic peak, as any other amplitude in the power spectrum, is very sensitive to both the ambient pressure and other external parameters, as it is the case for the microbubble concentration and the amplitude of the acoustic pressure transmitted at the point where the bubble resides. This is an important problem when looking at the medical applications of SHAPE, since it is not possible to determine the amount of the transmitted ultrasound signals that will be scattered while travelling through the tissue to the position of the microbubbles, and thus it is impossible to determine in a reliable way the acoustic pressure transmitted in that point.

In 2005, Adam *et al.* [66] and Ganor *et al.* [67] also explored the possibility of determining the ambient pressure by means of its relationship with the subharmonic and higher harmonics. Despite no conclusive results arose from their work, this is still of great interest, as they performed an exhaustive investigation on the theoretical and experimental characterization of the nonlinear bubble behaviour.

In general terms, as long as both the bubble concentration and transmitted acoustic pressure can be measured, this technique yields excellent results when determining the ambient pressure. However, its applicability into clinical cases might be limited, as its accuracy depends on factors that for the moment cannot be controlled in a real scenario.

Determination of the disappearance time of bubbles

This approach was first introduced by Bouakaz *et al.* [68] in 1999, and it is based on insonating microbubbles with a short duration high-intensity pulse, which destroys their shell and thus exposes the gas inside to the surrounding liquid. Then, the time needed for the bubbles to completely dissolve is measured, given that the rate of radius decrease of a bubble in a stationary liquid has a dependency on the ambient pressure, among other easy to characterize parameters, as demonstrated by de Jong *et al.* [69] in 1993. Nevertheless, errors of 50 mmHg are reported in their work, due to the difficulty of measuring the dissolution time accurately, which is little promising for medical applications, as the pressure changes needed to detect are of the order of 5 to 10 mmHg. This problem arises because the bubble radius decreases as a negative power-law of the time, which makes the determination of the moment when the bubble population has fully dissolved imprecise. In 2004, Postema *et al.* [70] carried out detailed numerical simulations assessing the eligibility of different microbubble filling gases for their use in the determination of the ambient pressure.

Dissolution time of microbubbles in blood is of the order of 20 to 40 ms, which, if compared to the cardiac period, which duration is of the order of one second, shows that this method could yield a good temporal resolution when performing pressure measurements inside the vascular system, since these times would allow for the achievement of several measurements within the period of interest. Nonetheless, if the aim is to measure the pressure at certain moments of the cardiac cycle, such as systole or diastole, it would not be possible to achieve a good time resolution, as these events take place in time periods of the order of 50 ms. Unfortunately, it is during these phases that pressure measurements are needed the most. In addition to this limitation, if bubbles are immersed in a flowing liquid (such as blood inside the vascular system) instead of a stagnant one, in order to properly determine the disappearance time of bubbles, convective and unsteady terms should be included into

the equations that characterize this behaviour. These terms are difficult to model and measure with the needed accuracy, which could also generate problems when aiming at obtaining precise results.

Characterization of the resonance frequency of microbubbles

When a bubble is insonated with an ultrasound wave with wavelength much larger than its diameter, the bubble behaves as a harmonic oscillator for a wide range of acoustic pressures. As stated before, the resonance frequency that characterizes this system is proportional to the square root of the ambient pressure [50]. Therefore, as first proposed by Fairbank & Scully [49] in 1977, by measuring the frequency at which the acoustic signal scattered by the bubble shows a maximum in the power spectral density, the pressure at its position can be obtained. In their work, it is shown a shift in the acoustic spectrum of bubbles in water as a result of a variation of 200 kPa in the ambient pressure. However, they did not perform a systematic study on the influence of the bubble properties on this effect. In 1987, Leighton [71] recorded the acoustic response of bubbles in water by means of an hydrophone, showing that the measured frequency corresponded to the one given by Minnaert [50].

The fist work to actually assess the exploit of this technique in medical applications was carried out by Bouakaz *et al.* [68] in 1999, who identified a series of accuracy issues. Finally, in 2010, Aldham *et al.* [72] conducted a systematic experimental study in which a single bubble was placed on a plate and the ambient pressure was varied by amounts of the order of 1 kPa, measuring the bubble resonance frequency. The Minnaert frequency formula was modified in order to take into account the effects derived from the presence of the plate. They showed that the resonance frequency of the bubble changes linearly with these pressure variations, despite of the fact that their pressure estimations showed some discrepancies with the real ambient pressures.

In addition to all the above described, in 2005, Adam *et al.* [66] and Ganor *et al.* [67] performed experiments using commercial UCA's, which physical properties cannot be changed, and sometimes not even measured with the needed accuracy. In must be pointed out that, despite of including the work of Adam *et al.* and Ganor *et al.* in the current subsection, the experiments they performed are based on the approach consisting in measuring the subharmonic peak amplitude, discussed in the first subsection of this section. Nonetheless, as the problems derived from the change in the dynamic behaviour of UCA's due to the shell properties are common to both approaches, their discussion is developed here.

The microbubbles shell affects the behaviour of UCA's by increasing their resonance frequency by about to 50%, according to Van der Meer *et al.* [73]. Thus, several

equations that take into account the effect of this coating on the bubble dynamics have been proposed in the literature, although for their applicability into real scenarios properties such as shell viscosity and elasticity would need to be measured, which constitutes a difficult task. Nevertheless, steps towards the development of UCA's with on-demand shell properties very well characterized and high monodispersity have been taken in the last years [74, 75].

1.3. Hypothesis and Experiment Description

The aim of this thesis is to study the acoustic behaviour of bubbles embedded in a viscoelastic material, in order to assess the feasibility of a technique to measure the ambient pressure based on the dependence of the bubble resonance frequency on such pressure. The intended application of this technique is the noninvasive measurement of pressure in points of difficult access inside the human vascular system.

As it can be deduced from the Minnaert's resonance frequency formula described in page 9, the size of the bubble and the ambient pressure determine at which frequency the bubble will exhibit a peak in the amplitude of its radial (i.e. volume) oscillations while being insonated with a pressure wave. Therefore, and given that the bubble size is know, by detecting this peak, it could be possible to determine the ambient pressure, as the rest of the parameters in the equation can be, in principle, characterized. For this purpose, we create millimetric air bubbles in a gelatin phantom, used as an experimental model of soft tissue [76], and apply a pressure wave on them, measuring the bubble frequency response by recording its behaviour with a high-speed camera. The type of acoustic wave to be used is known as a chirp, a pulse that covers a range of frequencies [77], in order to create a continuous frequency spectrum. The same measurements are performed for different bubble sizes and ambient pressures. The results obtained are also compared, albeit in a qualitative manner, with theoretical simulations of the bubble response under the aforementioned chirp insonation.

The main reason for choosing the approach based on detecting the shift in the bubble resonance frequency, instead of the other two approaches described in section 1.2, is that we consider this quantity as more prone to be detected with the accuracy needed to perform measurements within the vascular system. This is because, in order to efficiently detect small changes in the ambient pressure, it would be necessary to employ UCA's with a soft and elastic shell, as the stiffer the coating shell is, the less sensitive the microbubbles are to pressure changes. These UCA's with an elastic coating are also more sensitive to the insonating pressure wave amplitude, which can induce nonspherical volumetric oscillations in the bubbles (Fig. 7) when it exceeds a

certain intensity, and even provoke the collapse of the bubbles. These effects influence the harmonic response detected, generating peaks at unexpected frequencies and producing noise in the signal. Although these behaviours do not need to be taken into great consideration when employing US for imaging, it is key to avoid them when the purpose of the recorded signal is the analysis of its frequency components. Thus, it is considerably difficult to insonate the bubbles with a transmitted pressure which amplitude is high enough to reach the nonlinear regime, but at the same time low enough to avoid the nonspherical oscillations and collapse of the bubbles. This difficulty is remarkably higher when the objective is to perform these measurements *in vivo* using commercial UCA's, which properties are difficult to model due to their polydispersity, and it is impossible to know with exactitude the intensity of the transmitted pressure at the point of interest. Thus, we consider as more convenient to insonate the bubbles at transmitted pressures lower than the ones typically employed for US imaging, keeping this way their behaviour in the linear regime, and detect the fundamental frequency component instead of other harmonics.

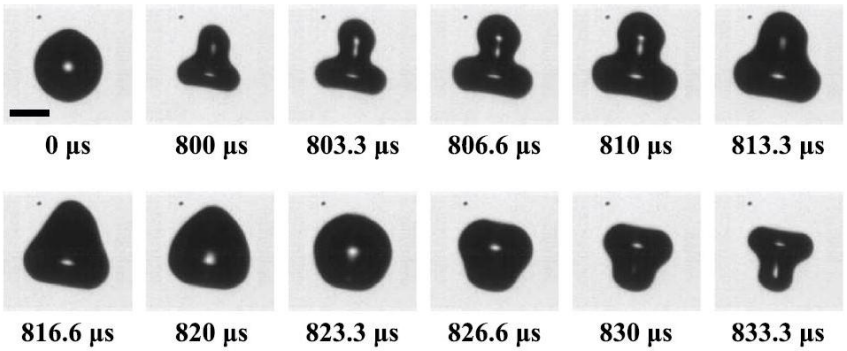

Figure 7. Nonspherical volumetric oscillations observed during insonation of microbubbles at high power (scale bar represents 100 µm) [78].

In addition to this reasoning, it is not unusual that the fundamental component of the recorded signal overlaps with the subharmonic and second harmonic components (Fig. 8). This creates the need of filtering the fundamental frequencies (the ones inside the grey rectangle in the image) with a high-pass filter (in case the measurements are performed using the second harmonic) or a low-pass filter (in case of using the subharmonic), which also suppresses part of the harmonic component information, reducing this way the accuracy of the measurements.

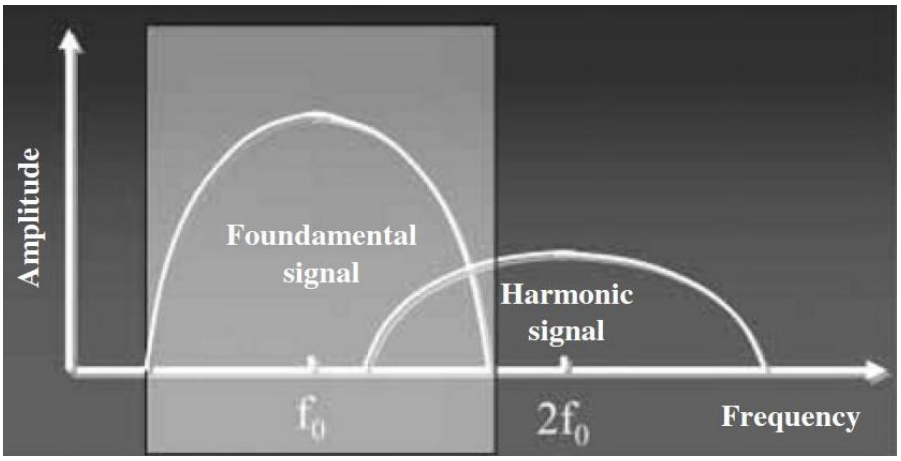

Figure 8. Schematic representation of the fundamental frequency component overlap with the second harmonic component, and of the required filtering step [8].

Moreover, we believe that the approach considered in this thesis could be easily implemented with the currently existing US imaging techniques. Extended pure harmonic detection (ePHD) is an US technique characterised by the transmission of a very low-transmit power pulse with frequency equal to the resonance frequency of the UCA's. This technique records information only from the fundamental harmonic and has been shown to have high sensitivity [8]. This technique is highly similar to the methodology employed for this approach, and thus it could be adapted to detect the frequency at which the signal scattered by the UCA's exhibits a greater amplitude. Given that the employed UCA's size can be presumably characterized in advanced, the difference between this detected frequency and the theoretical one for the UCA's size would allow the computation of the ambient pressure.

It should be noticed that the relatively large size of the bubbles used in this work is motivated by limitations in our experimental equipment, as described in section 4 (*Experimental Setup and Procedure*). Nonetheless, as this study focuses on the Physics behind the technique, the procedure could be easily translated to smaller bubbles (micron-sized, as used in medical applications) once the appropriate equipment becomes available. Moreover, we believe that the experiments performed in a single bubble could be easily extrapolated to a population of bubbles, as it would be the case when employing UCA's. *In* vivo, mutual interactions between microbubbles can be neglected and the acoustic response of a population of microbubbles can be estimated by summing up the individual responses of single bubbles [79], neglecting multiple scattering effects. In addition to this, the aforementioned problems with the polydispersity of UCA's populations could be addressed using the new manufacturing techniques that provide microbubbles with on-demand properties and high monodispersity [74, 75].

The choice of gelatin instead of a liquid as the surrounding medium has the main purpose of simplifying the acquisition of measurements, since the bubble will remain

at a fixed location at all times [78]. But more importantly, gels are broadly employed in the biomedical field due to the similarities between their properties and those of soft tissues like the ones found in muscles, heart or liver (Table 2.) [76]. Moreover, a bubble entrapped in a gel resembles the behaviour of a bubble inside a small capillary (with a radius not much larger than the one of the bubble) where the surrounding soft tissue would act in a similar way as the gelatin in this experiment.

Material	G (atm)
Gelatin solution	0.083–0.434
Gelatin solution	0.0002–0.0004
Gelatin/agar	0.07
Neural retina	$\sim 9.87 \times 10^{-4}$
Liver	0.001–0.003
Liver (bovine)	0.10
Liver	0.001
Heart	0.001
Fat (porcine)	0.46
Breast (turkey)	0.10
Limb	0.01
Muscle	0.005–0.010
Articular cartilage	0.33–5.26
Knee cartilage	2.0–4.0

Table 2. Shear modulus for different soft materials [76].

Regarding the bubble insonation technique, as a first approach we used pressure waves with a fixed frequency that were generated using a piezoelectric transducer (in a similar way to the experiments performed by Hamaguchi & Ando [78]). The bubble behaviour was recorded for a set of waves with different frequencies and for different ambient pressures. Nevertheless, this technique proved to be inefficient in terms of time and accuracy. The large number of experiments needed to characterize the bubble behaviour for a single ambient pressure (and consequently the time needed to perform these measurements in the same bubble at several ambient pressures) lead to changes in the bubble medium. These variations were evidenced by a slow vertical drift exhibited by the bubbles, as the gelatin slowly infiltrates with water from the surroundings and starts to lose consistency, which results in bubble displacement.

As an alternative, we moved on to the current approach of insonating the bubbles with a chirp (Fig. 9). This decision was made for several reasons. The first one is the time efficiency of this method, which allows for a large number of measurements before the conditions in the bubble medium change. Also, it is important to notice the strong potential of this technique to be applied to real clinical scenarios, as it holds a strong resemblance with the current US insonation techniques in terms of time and execution. Nonetheless, the most important reason is that the chirp covers a selected frequency spectrum in a continuous manner in one insonation, which allows for the detection of the resonance frequency of the bubbles even if this is not known in advanced. This greatly contrasts with the previous method, which required a large

number of separate measurements to achieve a discrete coverage of the range of frequencies of interest.

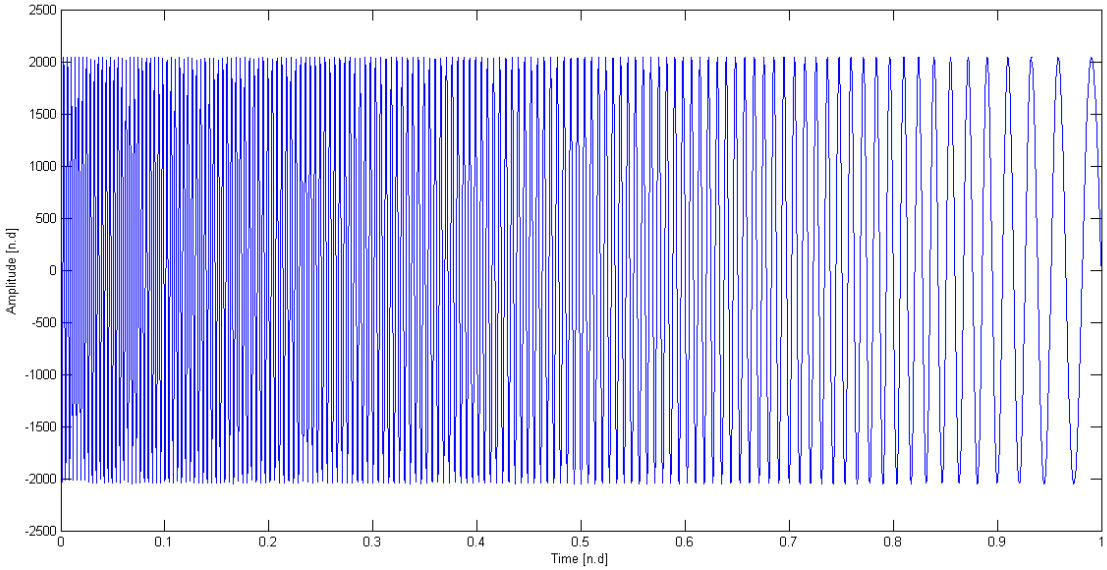

Figure 9. An example of one of the chirps programmed for the waveform generator, covering frequencies from 6 kHz to 1 kHz.

2. Theoretical Background

The Rayleigh-Plesset equation

The dynamics of an uncoated free bubble in a liquid was first described by Rayleigh in 1917 [80] and later modified by Plesset [81]. After undergoing several refinements over decades, the following equation was obtained, which is known as the Rayleigh-Plesset equation,

$$\underbrace{\rho\left(\ddot{R}R+\frac{3}{2}\dot{R}^2\right)}_{(1.1)}=\underbrace{\left(P_0+\frac{2S}{R_0}\right)\left(\frac{R_0}{R}\right)^{3\kappa}}_{(1.2)}\underbrace{\left(1-\frac{3\kappa\dot{R}}{c}\right)}_{(1.3)}\underbrace{-P_0-P_\infty(t)}_{(1.4)}\underbrace{-4\nu\rho\frac{\dot{R}}{R}}_{(1.5)}\underbrace{-\frac{2S}{R}}_{(1.6)}, \qquad (1)$$

where ρ is the liquid density, ν the kinematic viscosity of the liquid, c the speed of sound in the liquid, S the surface tension of the gas-liquid system and κ the polytropic exponent of the gas inside the bubble. P_0 is the ambient pressure and $P_\infty(t)$ the applied acoustic pressure, which wavelength is assumed to be much larger than the bubble diameter. R_0 is the initial bubble radius and R the time varying radius of the bubble, which changes with the volumetric oscillations. Spherical symmetry is assumed. The gas content of the bubble is kept constant and the bubble is assumed to be in an infinite medium.

The term (1.1) of the equation stands for the inertia generated in the surrounding medium by the bubble oscillations. The term (1.2) describes the pressure of the gas inside the bubble, while the (1.4) represents the sum of all the pressures acting on the bubble surface, both ambient pressure and the time-varying pressure of the sound field. The term (1.3) stands for the acoustic radiation damping through sound radiated away from the bubble, which will not be considered in the following equations described in this thesis as the range of frequencies employed is not high enough to take into consideration such effects. The term (1.6) characterizes the surface tension, which, although considered in following equations, is not an important contribution, since the radius of the bubbles analysed in this thesis are far too large for surface tension to play a big role in their dynamics. Finally, the term (1.5) describes the viscous damping of the surrounding medium, which governs the damping of the bubble volumetric oscillations.

Nonetheless, despite of this being one of the most commonly used equations to describe the dynamics of microbubbles insonated with US waves [82], it must be modified for the case concerning this thesis. Since bubbles are embedded in a gel medium, the viscous damping forces must be adjusted to take into consideration the viscoelastic properties of the gelatin. For doing so, we consider the Voigt model for

viscoelastic materials (which can be represented by a purely viscous damper and a purely elastic spring connected in parallel), as Hamaguchi & Ando [78] do in their work, which results into the following equation,

$$\underbrace{\rho\left(R\ddot{R}+\frac{3}{2}\dot{R}^2\right)}_{(2.1)}=\underbrace{\left(P_0+\frac{2S}{R_0}\right)\left(\frac{R_0}{R}\right)^{3\kappa_{eff}}}_{(2.2)}-\underbrace{\frac{2S}{R}}_{(2.3)}+\underbrace{3\int_R^{\infty}\frac{\tau_{rr}}{r}dr}_{(2.4)}-\underbrace{\left(P_0+A\cos(2\pi ft)\right)}_{(2.5)}, \qquad (2)$$

The term (2.5) accounts for the pressure wave that generates the bubble oscillations, where A is its amplitude (assumed small), and f is the sound's frequency. The spatial integral of radial stress tensor, τ_{rr}, is evaluated using the Voigt model [83],

$$3\int_R^{\infty}\frac{\tau_{rr}}{r}dr=-\frac{4\mu_{eff}}{R}\dot{R}-\frac{4G}{3}\left[1-\left(\frac{R_0}{R}\right)^3\right], \qquad (3)$$

where G is the rigidity of the gel (one third of the Young modulus for incompressible cases). It should be pointed out that κ_{eff} and μ_{eff} are the effective polytropic index and viscosity, respectively [78], which account for the viscosity damping and compressibility of the gelatin, and heat conduction at the bubble wall.

As the amplitude of the driving pressure is kept low enough for the bubble behaviour to stay in the linear regime during the experiments, generating small-amplitude volumetric oscillations, equation (2) can be linearized. For this purpose R can be stablished as $R = R_0(1 + x(t))$ for $|x| \ll 1$, and equation (2) can be rewritten as

$$m\ddot{x}+c\dot{x}+kx=A\cos(2\pi ft), \qquad (4)$$

where

$$m=\rho R_0^2, c=4\mu_{eff}, k=3\kappa_{eff}\left(P_0+\frac{2S}{R_0}\right)-\frac{2S}{R_0}+4G.$$

Assuming the steady-state condition, the solution to equation (4) is

$$x(t)=X\cos(2\pi ft+\delta), \qquad (5)$$

where the amplitude X stands for

$$X=\frac{A/k}{\sqrt{\left[1-(f/f_N)^2\right]^2+4\zeta^2(f/f_N)^2}},$$

and the phase shift,

$$\delta = \arctan \frac{2\zeta(f / f_N)}{1-(f / f_N)^2},$$

being f_N the natural frequency of the bubble, and ζ, the damping ratio, which are defined as follows,

$$f_N = \frac{1}{2\pi}\sqrt{\frac{k}{m}}, \quad \zeta = \frac{c}{2\sqrt{mk}}. \tag{6}$$

It should be pointed out that the closer the frequency of insonation (f) is of the fundamental frequency of the bubbles (f_N), the larger the amplitude of the oscillations will be, exhibiting resonance.

Bubble resonance frequency dependency on pressure

As developed above, the resonance frequency of a bubble embedded in gelatin is determined by the following equation,

$$f_N = \frac{1}{2\pi}\sqrt{\underbrace{\frac{3\kappa_{eff} P_0}{\rho R_0^2}}_{(7.1)} + \underbrace{\frac{2S(3\kappa_{eff}-1)}{\rho R_0^3}}_{(7.2)} + \underbrace{\frac{4G}{\rho R_0^2}}_{(7.3)}}, \tag{7}$$

where it can be clearly seen that the bubble fundamental frequency depends on its equilibrium radius, the ambient pressure, the surface tension, the effective polytropic index, and the rigidity and density of the gel. The term (7.1), that stands for the effect of the ambient pressure in such frequency, is the one accounting for the greatest contribution to this value.

As it can be deduced from equation (7), while not modifying the medium properties and having characterised the constants (S, G, ρ, κ_{eff}), any variation in the bubble resonance frequency depends exclusively on its size and ambient pressure.

In addition to this, if we take into consideration the Ideal Gas law, it is obtained that the bubble radius changes depending on the ambient pressure. Putting together these two ideas, one can develop an equation that determines an unknown ambient pressure based on measurements performed at some reference conditions and the resonance frequency obtained experimentally.

For the sake of simplicity, the development of this equation will be carried out using the Minnaert's frequency formula instead of equation (7), as both yield similar results. Despite of this, the measurements performed while analysing the experimental data were carried out considering the Voigt-adapted equation.

We consider the Minnaert's resonance frequency

$$\omega_0 = \sqrt{\frac{3\gamma P_0}{\rho R_0^2}}, \tag{8}$$

where γ is the adiabatic index (which for isentropic oscillations equals κ = 1.4). P_0 is the ambient pressure at the bubble's location, and R_0 the equilibrium bubble radius. From the ideal gas law we obtain: $P_0 R_0^3 = (P_0 + \Delta P) R_1^3$, where P_0 is the initial pressure at some reference conditions where the bubble radius is R_0. Following this equation, if the bubble is compressed isothermally by an amount $\Delta P \ll P_0$, its new resonance frequency (namely ω_1) will be given by

$$\omega_1 = \sqrt{\frac{3\gamma P_0}{\rho R_0^2}}\left(1+\frac{\Delta P}{P_0}\right) = \omega_0\left(1+\frac{\Delta P}{P_0}\right). \tag{9}$$

This equation shows that the resonance frequency of a bubble varies linearly with the relative overpressure $\Delta P/P_0$. Therefore, knowing the new resonance frequency it would be possible to determine the pressure that surrounds it.

Numerical simulations

In order to perform qualitative comparisons between the experimental results and the theory, a numerical simulation was implemented. This simulation was created considering equation (2), which describes the change in the bubble radius amplitude with time. To perform the numerical integration of the Rayleigh-Plesset equation we have used the routine *odeint*, implemented in the library SciPy of Python, and that is based on the library LSODE, widely used in the scientific community. The simulation allows for the computation of the dynamics of hypothetical bubbles under insonation with a chirp (Fig. 10 (a,b)). These simulations have been performed for bubbles of several sizes and for a range of ambient pressures. By determining the peak in the frequency spectrum by means of a Fourier analysis for each set of conditions (employing the routine *welch* from the SciPy library) (Fig. 10 (c)), a plot where the hypothetical resonance frequency shift due to pressure variations is obtained (Fig. 11). This was used as a guide when programming the experimental chirp, in order to set a range of frequencies suitable for the expected resonance frequency of the bubbles analysed.

Moreover, the implementation of this program also allows for a simulation of the bubble behaviour in response to the experimental chirp (i.e. the signal recorded with the pressure sensor), instead of the idealised chirp, in order to carry out a better comparison between theory and experimental results.

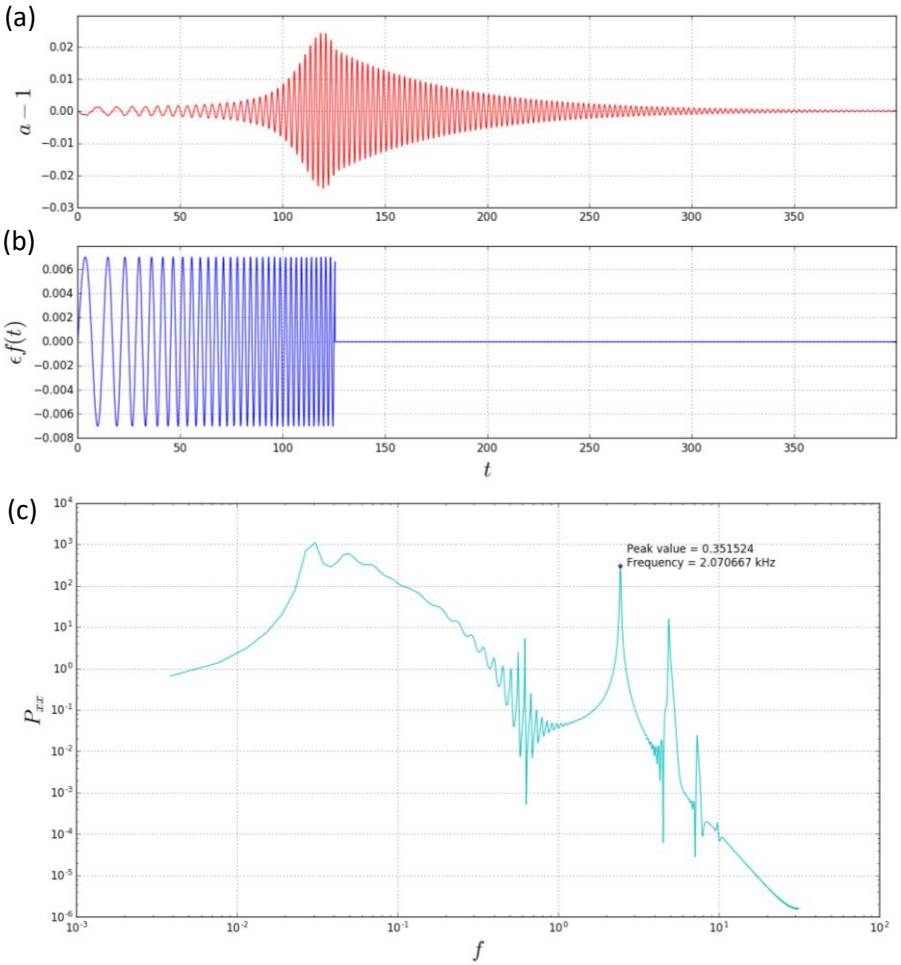

Figure 10. Simulated radius response over time (a) for a bubble of 2.6 mm in diameter to insonation with the theoretical chirp depicted in (b). Both are dimensionless and thus, the graphs have no units. Fourier analysis of the bubble radius variation over time is shown in (c).

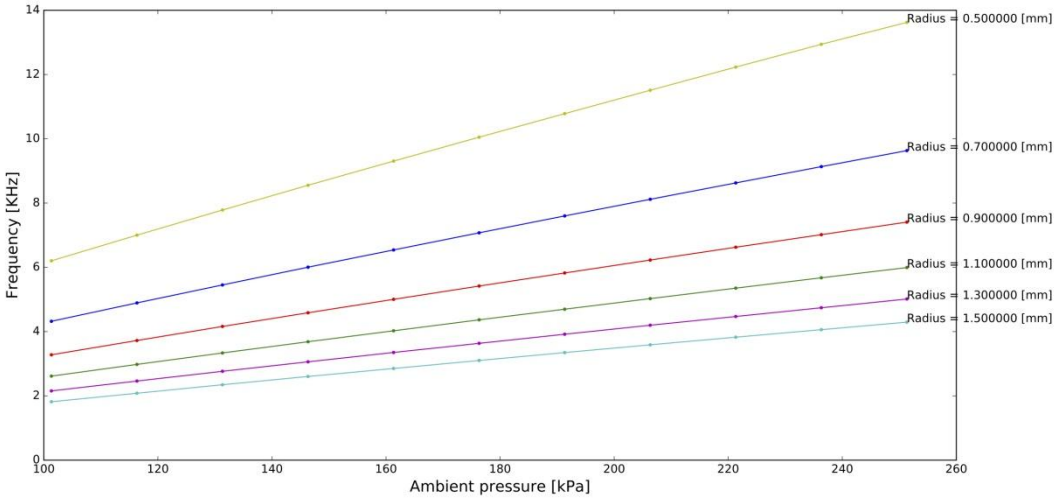

Figure 11. Theoretical resonance frequency shift due to pressure variations, computed for different bubble sizes.

To characterize the bubble dynamics, it was assumed that the density of the gel and the speed of sound in the medium are equal to the ones in water. The surface tension considered is the one for the water-air interface. For the unknown values of the rigidity and viscosity of the gel, we considered the values proposed by Hamaguchi & Ando in their work [78], which were obtained from the fitting of their experiments to the linear theory. This decision is based in the fact that they employ the same porcine gelatin that we use in our experiments, and in a concentration very similar to ours.

Finally, in order to determine the polytropic index to be used in the simulations, an analysis of the bubble thermal boundary layer was carried out. We considered the two possible limit situations where the combination of bubble radius and insonation frequency could lead to an isothermal behaviour, and compared the results with the values proposed by Prosperetti [84]. The polytropic index value was estimated to be very close to 1.4 (adiabatic index) in both scenarios, which allows us to consider the bubble oscillations as an isentropic process.

3. Objectives

This thesis comprises the following objectives:

- To design and implement an experimental protocol to measure the resonance frequency of a gas bubble immersed in gelatin. This protocol shall include:

  - Preparation of gelatin samples of suitable properties.
  - Programming and synchronisation of the different lab equipment (function generator, high-speed camera, acquisition system, etc).
  - Implementation of an advanced image-processing algorithm to accurately measure bubble oscillations of amplitude smaller than one pixel (sub-pixel resolution).
  - Development of advanced signal processing tools, based on wavelets, to post-process both pressure and radius signals.

- To prove experimentally the feasibility of using this resonance frequency to determine the ambient pressure.

- To implement the numerical integration of the equations describing the volume oscillation of the bubble, in order to develop a tool that will serve us as a guide to optimise the methodology in the future.

4. Experimental Setup and Procedure

4.1. Gelatin Preparation Protocol

In order to produce the gelatin phantom, used as an experimental model of soft tissue, Type-A gelatin from porcine skin (G2500 Sigma-Aldrich) is mixed with heated deionized water in a proportion of 2 g per 100 ml of water. The mixture is then stirred until the perfect dissolution of the gelatin and poured into a cylindrical transparent LDPE (Low-density Polyethylene) flask of 30 mm in height and 15 mm radius. The container is stored at 3 ^{o}C overnight, allowing for the solution to gel.

The concentration used was determined by trial-and-error to be the most suitable one for the experiments performed in this thesis. It allows for bubbles to be generated and trapped inside the gel, and for the pressure waves emitted by the transducer to reach these bubbles. All this without a significant loss of structural consistency during the time needed to perform the experiments. The reference gel strength is 250 g Bloom, according to the Bloom gelometer test. Nevertheless, since this is a measure for the concentration typically used for this test, it is impossible with the available resources to determine accurately the viscosity that corresponds to the concentration used in these experiments. The gelatin density is assumed to be the same as that of water.

4.2. Bubble Generation Protocol

Bubble generation through a high-power laser pulse

The first approach used in this work to generate bubbles inside the gelatin phantom consisted in focusing a laser pulse inside of it at a certain focal distance. The pulse is generated using a high-power Nd-YAG (Neodymium-doped Yttrium Aluminium Garnet) laser (CFR400, Big Sky Laser Quantel) that emits a 532 nm beam of up to 200 mJ during 8 ns sent through a 30mm focal distance biconvex lens towards the gel. At the focusing point the gelatin temperature increases very quickly, causing a small explosion that generates a cavity due to the diffusion of the dissolved air inside the gel. After the initial burst, this air cavity then compresses and expands repeatedly following the Rayleigh-Plesset equations, diminishing its size until eventually a spherical micron-sized bubble is generated. Fig. 12 shows this process for a laser pulse of 70% of the maximum laser power.

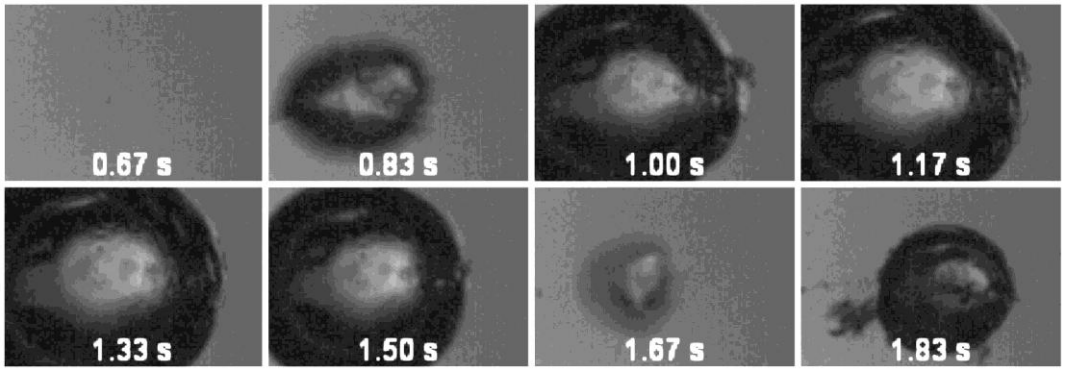

Figure 12. Bubble formation after a laser shot at 70% of the maximum laser power. The generated bubble exhibits volumetric oscillations until it establishes at its equilibrium size.

The size of the resulting bubbles can be tuned by modifying the power of the pulse. Despite of this, it was observed that for pulses with a power larger than 80% of the maximum power the burst generates a cloud of bubbles instead of a single one. Pulses of 70% or lower generate bubbles of approximately 100 µm radius or less, which should exhibit resonance at frequencies of 28 kHz or higher, according to the Minnaert's equation. Since the available piezoelectric transducer for these experiments is set to operate in a range of frequencies between 1kHz and 10kHz approximately, which are far below the frequencies needed to observe any resonance in the bubbles generated using a laser pulse, this approach resulted unviable for the purpose of this thesis and was discarded.

Bubble generation through direct air injection

An alternative approach to generate bubbles in the desired range of sizes consists in directly injecting air in the middle of the gel through an epidermic needle of 425 µm of radius. This procedure is less repeatable than the laser-based one, but was found to be the only one capable of generating quasi-spherical bubbles of the suitable sizes.

After the removal of the needle it was observed that the gelatin above the bubble is resealed, which creates a proper scenario for the experiments, where the bubble is suspended in the gel and apart enough from other bubbles, so its behaviour cannot be influenced by any external feature.

4.3. Gel Insonation and Experimental Setup

The flask containing the gelatin, where air bubbles were previously generated, is introduced inside a pressurized steel chamber (which dimensions are 10 x 4 x 3.5 cm) and fixed using a support 3D-printed in ABS, which was especially designed for this

experiment. The chamber (custom-made by Vázquez y Torres Ingeniería, S.L.) is then closed and filled with deionized water previously degasified. At the chamber bottom there are two sensors. One measures the ambient pressure inside the chamber (3100 Series Pressure Transducer, Gems Sensors & Controls), which can be easily modified in a progressive way via a regulation valve connected to a pressure line. The other sensor (Model 2013D, DYTRAN INSTRUMENTS INC.) records faster changes in pressure, such as the acoustic wave generated to make bubbles oscillate. At the top of the chamber there is a piezoelectric transducer (PSt 1000/16/40 VS25, Piezosystem jena Gmbh) that is in charge of producing the pressure waves. A silicone film is glued to the cap of the chamber in order to perfectly seal the cavity, leaving only a small hole at its centre to screw the piezoelectric actuator (a brass disk of 2 cm radius used to transfer the piezoelectric movement and generate the pressure wave) so that this is in direct contact with water. The purpose of this film is to keep the water volume inside the chamber constant in all the experiments, as it was observed that modifications in the water level due to changes in the ambient pressure affect the wave generated by the transducer.

The acoustic pulse is produced by a waveform generator (Model DS345, Stanford Research Systems) controlled by a Matlab code used to implement the chirp, and that sets the initial and final frequency along with its amplitude. The chirp duration is 8 ms and its range of frequencies varies depending on the experiment. The signal is modulated so that its amplitude grows and decreases progressively at its beginning and end respectively, softening this way the initial and final vibrations of the piezoelectric and producing a clearer signal. It is subsequently amplified (LE 200/300/EBW, Piezomechanik GmbH) and sent to the piezoelectric transducer, which vibrates and transmits the acoustic pulse to the chamber interior. An electrical trigger is also set, in order to synchronise the emission of the acoustic wave with the camera and sensors recordings.

The bubble behaviour is recorded through a window in the front side of the pressurized chamber with a high-speed camera (Memrecam HX-3, nac) at 40,000 frames per second (which is at least three times the Nyquist sampling rate for the highest frequencies used) setting the exposure time to 25 µs and with a spatial resolution of around 20 µm per pixel, although the exact value depends on the experiment. A 55mm Nikon lens, equipped with an extension ring of 36 mm, was used to record the bubbles, and a window of 512 x 384 was employed in most of the experiments. A light source is placed on the opposite side of the pressurized chamber so that it backlights the bubbles inside the gel, recording them as a shadowgraph. Videos of 27.5 ms are stored, including recordings of 2.5 ms before the trigger is sent (and thus the chirp is emitted) and 17 ms after the transducer vibration ceases, ensuring this way that any possibly interesting event is filmed.

The trigger signal also establishes when the recordings from both pressure sensors are saved into a computer through an acquisition card (NI USB-6210, National Instruments) controlled by a LabVIEW program, keeping this way the actual acoustic waves emitted by the transducer and the current absolute pressure inside the chamber. The signal obtained from the high-frequency sensor is amplified by a signal conditioner.

Fig. 13 shows a diagram of the setup used to perform the experiments, representing all the connections among the equipment.

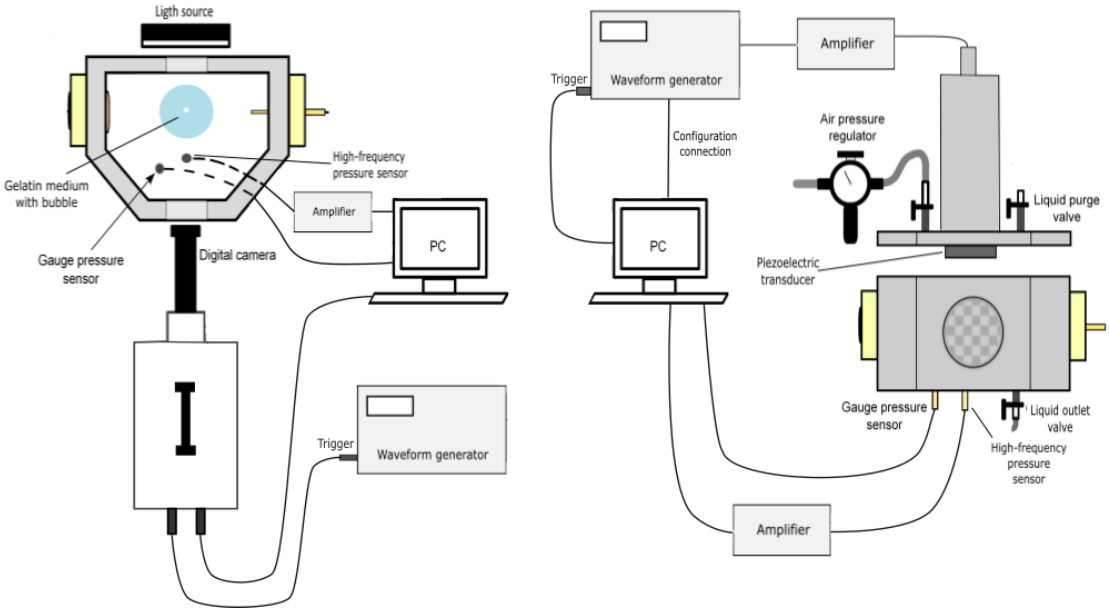

Figure 13. Implemented experimental setup.

4.4. Image Processing

The recorded videos are analysed using the image processing software Matlab. For this purpose videos are examined frame by frame in order to know the bubble radius and centre position for each image and thus track their changes with time. A threshold is established and pixels with a lower greyscale value (darker colour) are selected. Picking only the first and last selected pixels in each row a rugged bubble contour is obtained. In order to provide sub-pixel resolution, which is essential in this project due to the small amplitude of the bubble oscillations, a linear interpolation is applied between the pixels that constitute this primary contour and the pixels adjacent to them which values are above the threshold. The final values considered as the bubble border, instead of integer pixel numbers, are real numbers that correspond to the point where the interpolated exact threshold value is. A diagram of the algorithm is depicted in Fig.

14, including an example extracted from the analysis of one of the bubbles studied in our experiments.

The next step is to find the parameters that set a circle that best fits this contour, in order to obtain its radius and centre position. For this, the *fminsearch* function is used iteratively until the circle equation that best fits the bubble border is found.

A time evolution of the bubble radius and centre is displayed while the program runs (Fig. 15).

Regarding the uncertainty of the measurements, we have estimated the sub-pixel resolution of the image detection algorithm to be smaller than 0.06 pixels, based on the variability of the measurement for a constant-radius bubble. With the spatial resolution used in the experiments, this uncertainty accounts for around 1.2 µm, which allows for quite accurate results given the amplitude of the radius oscillations observed in the experiments.

(a)

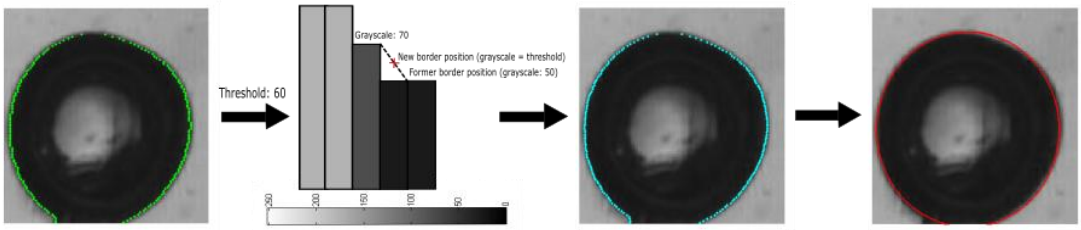

(b)

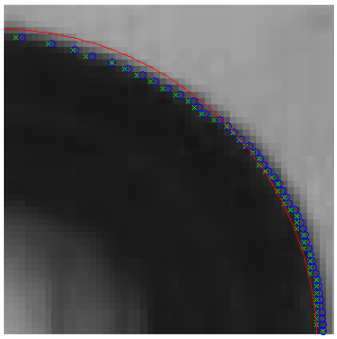

Figure 14. Diagram explaining the algorithm implemented for the bubble border detection. In (a) it is observed how the detected bubble contour changes after the interpolation step from a rugged border (green) to a softer one (cyan), leading to the fitting of a circle (red) to the contour. An amplified view of the different border characterization techniques is depicted in (b), being the green crosses the initial rugged border, the blue circles the sub-pixel resolution contour, and the red line the circular curve fitted to the interpolated contour.

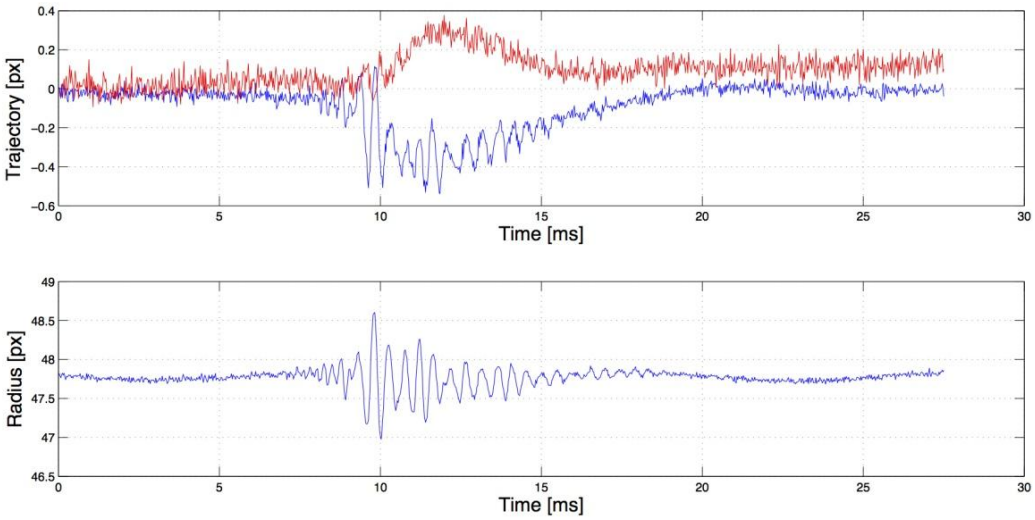

Figure 15. Example of the bubble centre trajectory (a) and radius amplitude variations over time (b). It must be pointed out that the red line in (a) shows the centre position changes in the x-axis while the blue line depicts this information in the y-axis.

4.5. Data Analysis and Frequency Response

In order to determine the resonance frequency at which the recorded bubbles are oscillating it is required an analysis of their frequency spectrum. A Fast Fourier analysis is performed on the radius amplitude variations obtained with the image-processing algorithm described in the previous section. This analysis is carried out in Matlab using the built-in function *fft*, and the frequency spectrum is displayed.

A more thorough examination is performed on both the pressure signal recorded with the dynamic sensor and the bubble radius variations. This is done by means of a wavelets analysis. For signals in which the frequency inherently varies quickly, such as a chirp, conventional analysis based on Fourier transform is not able to properly capture the frequency response of the system. For this reason we have adopted an approach based on wavelets that yields frequency spectra resolved in time [85]. The wavelet basis employed is the Haar sequence.

Wavelet analysis differs from Fourier analysis in that, while in Fourier the original signal is projected onto series of sines and cosines (both of infinite duration) which summation accounts for an approximation of the original waveform, in wavelets the original signal is projected onto series of functions that only extend for a finite time period. That is, functions localized in time and in frequency, not just in frequency, as is the case for Fourier bases. This type of analysis divides the signal into evenly-spaced time intervals, for which the power spectral density is computed. This yields a plot as the one observed in Fig. 16, where the strongest frequency contribution to the original signal over the time interval being analysed is represented in dark red, while

frequencies with smaller contributions at all are depicted in blue. For the simulated chirp shown in Fig. 16, it is clear that while the signal is not null, the main frequency descends over time following the red band circled in black[3] until the time when the signal suddenly stops, for which there is not a main frequency component, shown by a blue spectrum from that moment on.

The uncertainty in our pressure measurements due to the sensor is of 0.172 Pa, which corresponds to the resolution (equivalent electrical noise). As this value is so small compared with the measured ones, we assume this error as negligible and thus, we do not plot error bars in the pressure measurements.

Temporal errors in the acquired signals due to equipment performance are also negligible, as a consequence of the very fast response of both the camera and pressure sensor.

[3] This black oval was added in order to facilitate the explanation of the image, and it is not part of the original wavelet plot.

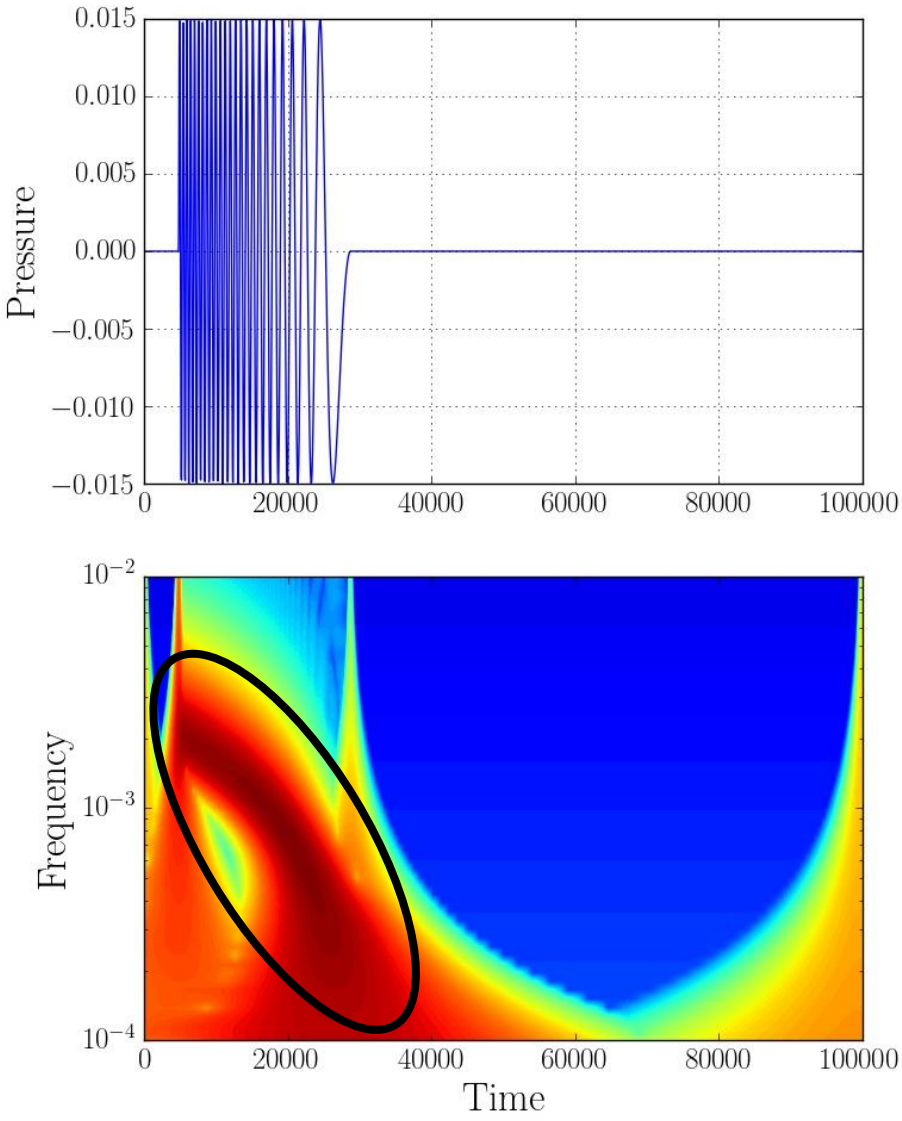

Figure 16. Display of a theoretical chirp (a) together with its wavelet spectra (b). In (b), the dark red band corresponds to the time evolution of the peak marking the central frequency of the signal. The two spikes that extend to very high frequencies at the beginning and end of the pulse are associated to the Gibbs effect, and is far less noticeable in real measurements, that start and end in a not-so-sharp way.

5. Results and Discussion

The experimental setup described in the previous sections is used to insonate the bubbles with a chirp. Experiments were performed for 10 different bubbles in different days. Nonetheless, for the sake of conciseness, in the following discussion we will focus on the set of experiments performed on the January 25th, 2017, summarized in the table below. This choice is motivated by the fact that a wider range of ambient pressures was covered that day, together with the better characterization of the experimental conditions. The chirp configuration was set to cover the range between 6 kHz and 1.5 kHz. The ambient pressure was varied non-monotonically between the different sessions in order to check that hysterisis effect did not influence the results obtained.

Session	Bubble radius at equilibrium [mm]	Ambient pressure [kPa]	Theoretical resonance frequency [kHz]
v1	1.345	101	2.127
v3	1.070	201	3.713
v4	1.205	151	2.873
v5	1.110	171	3.310
v7	1.055	181	3.580
v8	1.223	128	2.616

Table 3. Description of the conditions for each experimental session in the set of experiments performed January 25th, 2017.

The theoretical resonance frequency of the bubble at the measured ambient pressures was computed using the Voigt-model frequency formula (equation (7) from section *2. Theoretical background*). In order to demonstrate that the bubble size fulfils the Ideal Gas law, and correspondingly that pressures are measured properly, a comparison between the measured evolution of the bubble equilibrium radius with pressure and the corresponding theoretical values is depicted in Fig. 17. Moreover, a snapshot of the bubble at equilibrium (i.e. not being insonated) at the lowest and highest ambient pressure is shown in Fig. 18 in order to provide a visual assessment of the radius variation.

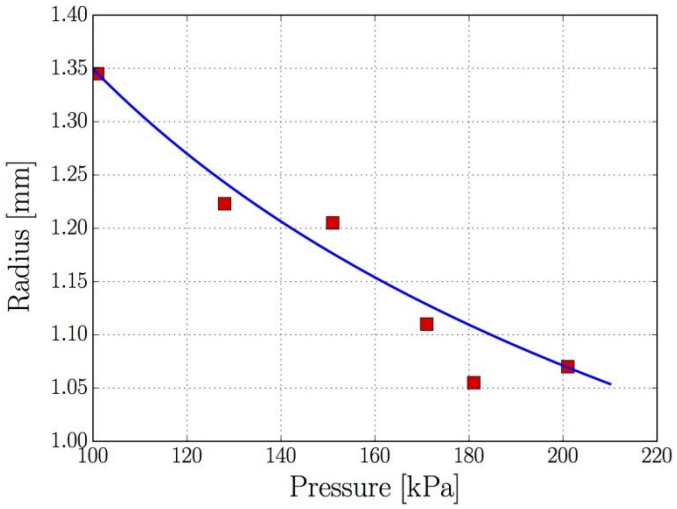

Figure 17. Experimental radius evolution with pressure in comparison to the theoretical values. The errors in the bubble sizes may be attributed to the non-sphericity of the bubbles, as can be appreciated in Fig. 31.

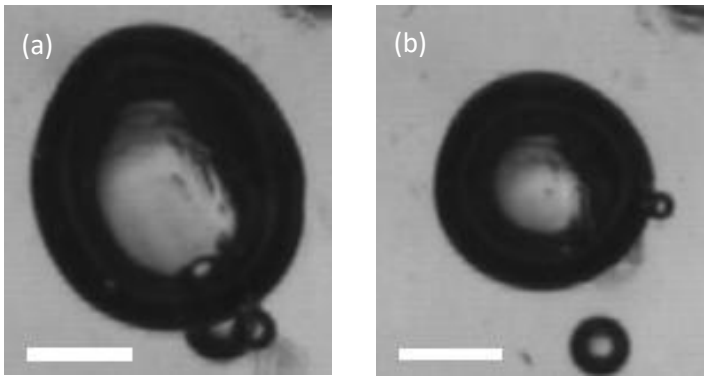

Figure 18. Snapshots of the bubble at equilibrium for an ambient pressure of approximately 101 kPa in (a) and of 201 kPa in (b). The scale bar represents 1 mm.

Numerical Results

We start our discussion by showing the simulated response of the bubble at two different pressures, 101 kPa and 201 kPa, corresponding to sessions v1 and v7. To show the idealised response we will use a theoretical chirp, presented in Fig. 16 in the previous section. Fig. 19 (a) and (c) show the time evolution of the bubble radius in response to this idealised pulse. Fig. 19 (b) and (d) contain the wavelet spectra for these simulations. The results are dimensionless and thus, the plots' axes have no units. From the comparison between both spectra, two conclusions can be drawn. Firstly, the resonance peak is located at a higher dimensionless frequency in Fig. 19 (d), and secondly, the start of the red band in the wavelet spectra corresponding to the time evolution of this peak starts earlier. This is consistent with the behaviour shown in Fig. 19 (a) and (c), where the maximum oscillation amplitude in the radius of the bubbles is achieved at an earlier time for the bubble at higher ambient pressure. This is

indeed the expected response, as the chirp sweeps from high to low frequencies and consequently, excites first the resonance of the bubbles withstanding higher pressures.

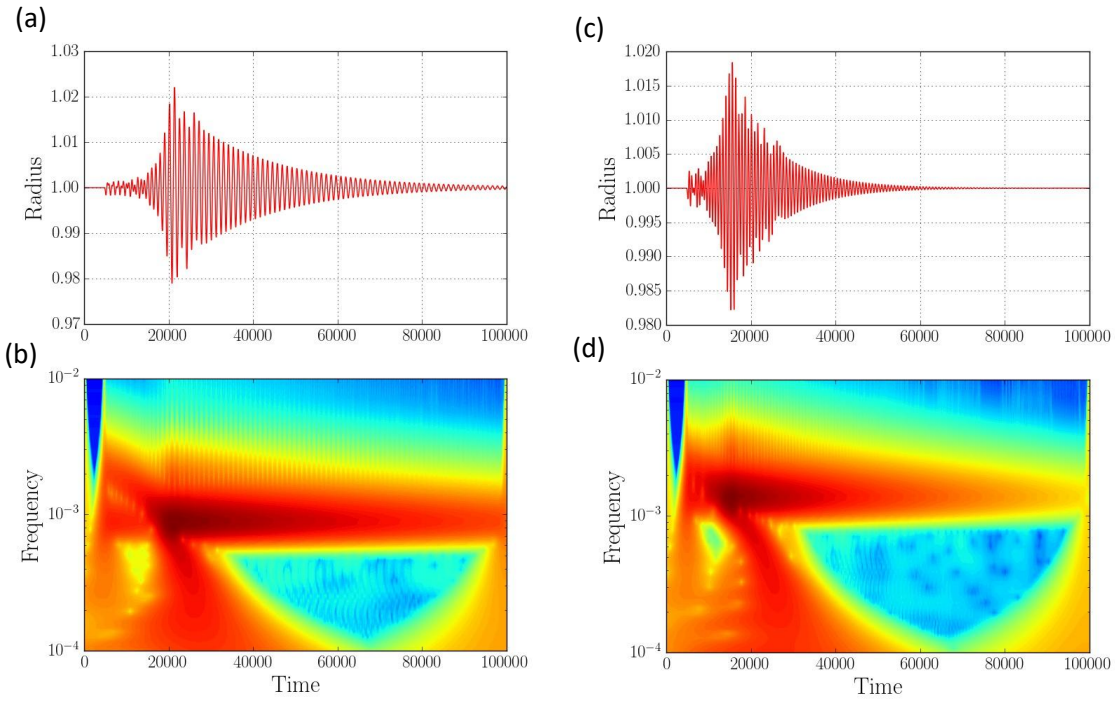

Figure 19. Simulated response of the experimental bubbles to an idealised chirp, computed for sessions v1 (a,b) and v7 (c,d), showing the bubble radius variation with time and its corresponding wavelet spectra.

The behaviour just explained is the expected one for our bubbles, if it was possible to accurately control the chirp.

Getting one step closer to the real situation, we will repeat the same simulations using the actual pressure pulses measured in experiments v1 and v7 (Fig. 20 (c) and Fig. 21 (c)) instead of the theoretical chirp. These simulated responses are shown in Fig. 20 (a) and Fig. 21 (a). Since the simulations are fed with actual measurements, which have units, these figures are shown in dimensional form. Unfortunately, the first difference between these figures and those associated to the idealised pulse is that the band that characterises the resonance peak evolution over time is not so manifestly different between the two simulations, showing a clear frequency component at around 2kHz in both spectra. This suggests that the pressure pulse experimentally measured does not allow for the resonance frequency to be detected clearly, as it will be demonstrated in the next subsection.

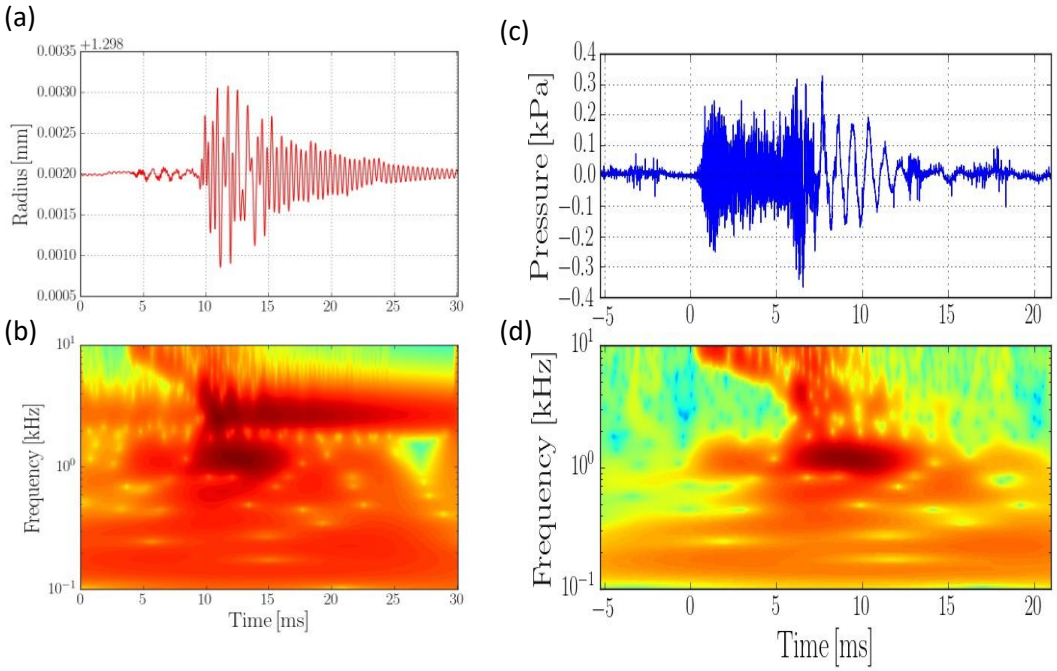

Figure 20. Simulation of a theoretical bubble response under the same conditions than in session v1 (a,b). Analysis of the experimental chirp measured for session v1 (c,d).

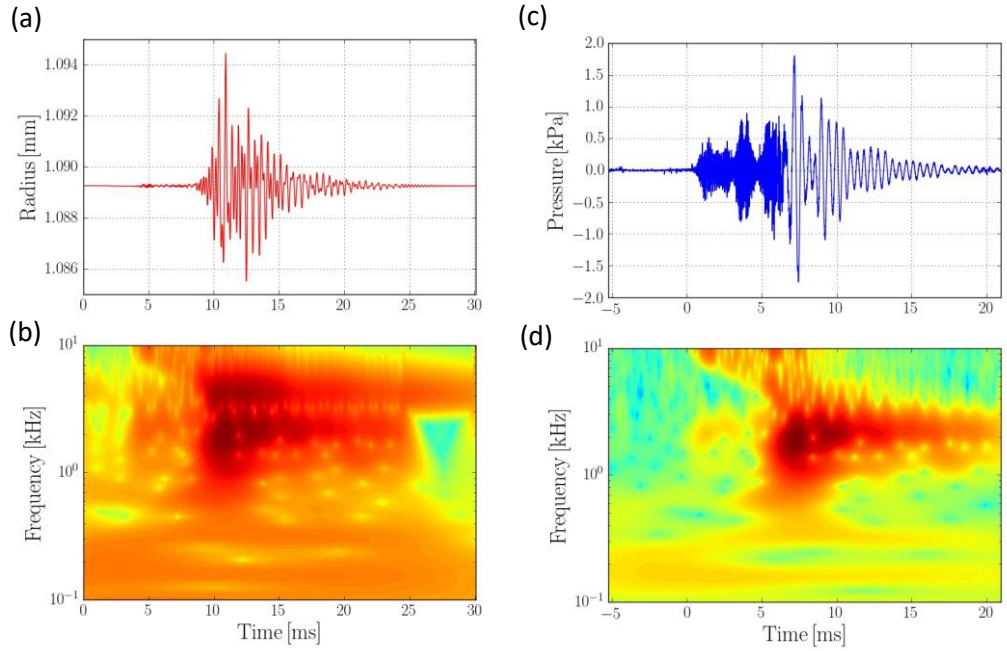

Figure 21. Simulation of a theoretical bubble response under the same conditions than in session v7 (a,b). Analysis of the experimental chirp measured for session v7 (c,d).

Experimental Results

In this section we report the experimental results corresponding to sessions in table 3. Fig. 22-27 (a,b) show the time evolution of the bubble radius measured experimentally for the different ambient pressures, alongside with its associated wavelet spectra. Moreover, Fig. 22-27 (c,d) show the pressure pulses measured for these sessions. As we could anticipate using the simulations described in the previous subsection, the bubble responses do not show significant differences in their spectra despite the relatively large pressure variations.

Fig. 22-27 (b) present a peak band clearly identifiable around 2kHz, which also turns out to be the dominant frequency in the piezoelectric transducer response. These results exhibit a strong resemblance with the simulations displayed in Fig. 20 (a,b) and Fig. 21 (a,b). The only remarkable difference between the experimental and simulated results resides in a second band appearing at higher frequencies in the case of the simulation for v7 (Fig. 21 (b)). This difference is a result of the much larger number of resolved points that the numerical analysis allows for, and that cannot be resolved for the experimental bubble response due to the limitations of the high-speed camera (it should be kept in mind that the movies are acquired at 40 kHz, whereas the simulation points are spaced about 0.3 μs, which would correspond to a sampling frequency of around 300 kHz).

It is clear from examination of the pressure pulses (Fig. 22-27 (c,d)) that the piezoelectric transducer is not able to follow the signal that the wave generator plus amplifier is sending (Fig. 28). As it can be observed in this figure, the shape of the chirp is clearly identifiable, and the peak frequency band in the wavelet spectrum is well defined, moving from high to low frequencies in a very similar manner to how the idealised chirp does. Had we have this signal coming out of the transducer, our simulations suggest that changes in the resonance frequency associated with ambient pressure variations should become noticeable with our experimental procedure and analysis techniques.

In fact, we are able to quantify accurately the main frequency at which the bubble oscillates, which unfortunately, in our experiments, is dictated more by the intrinsic behaviour of the piezoelectric transducer rather than by the bubble acoustical properties. Nonetheless, it should be pointed out that the measured frequencies are in the same range than the theoretical resonance ones (indeed, the expected resonance frequency for session v1 is around 2kHz, which corresponds also to the main frequency component measured from the piezoelectric response). This proves that the experimental setup and image analysis tools would be capable of resolving the bubble oscillations at the corresponding resonance frequency if the chirp obtained was the ideal one.

Thus, the discussion of these experiments allows us to conclude that the problem in the setup that prevents us from obtaining the desired results can be clearly identified as an issue in the piezoelectric response. Consequently, our goal now is to select a different one capable of operating properly in the range of frequencies of interest. This improvement in the facility, that is crucial to achieve the final objective of the research project, is currently underway at the moment of writing this dissertation.

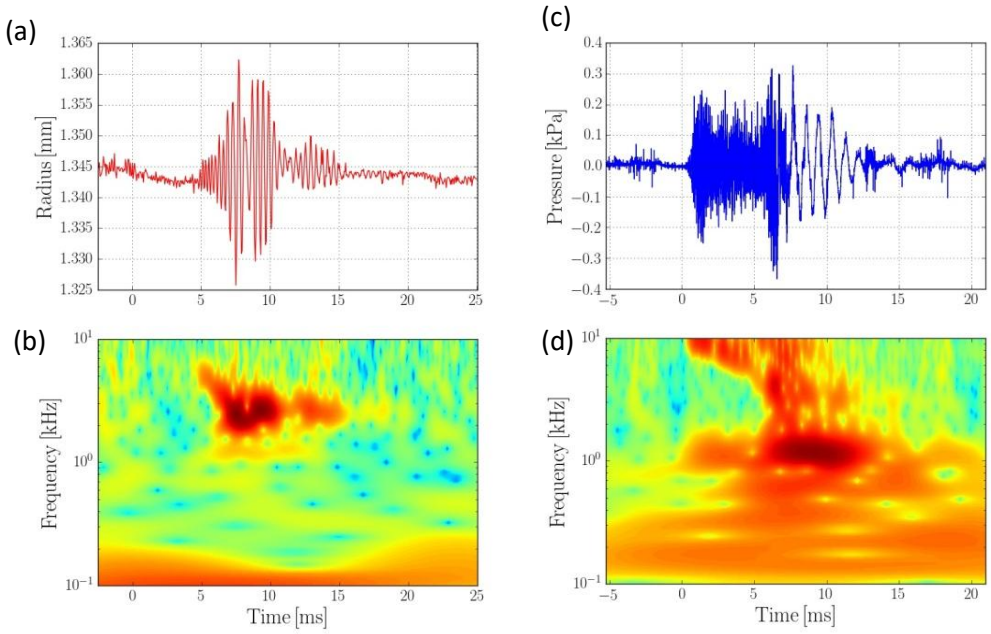

Figure 22. Results obtained for session v1. The bubble radius time evolution (a), together with the corresponding wavelet spectra (b) is displayed. The experimentally measured chirp insonating the bubble is also characterized (c,d).

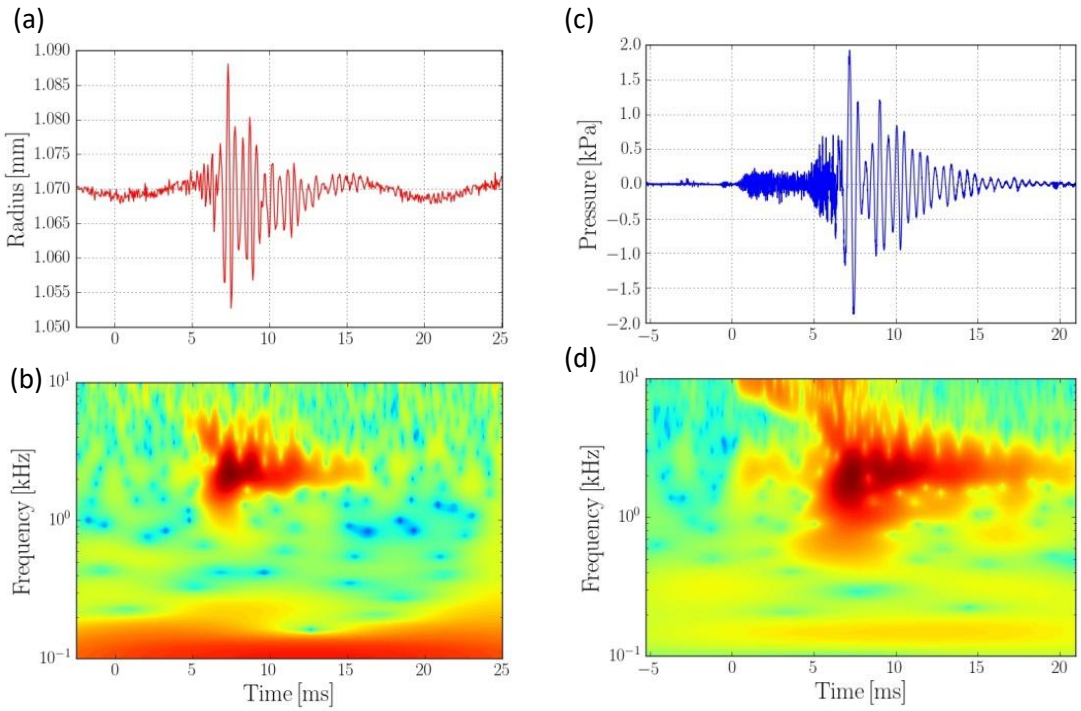

Figure 23. Results obtained for session v3. The bubble radius time evolution (a), together with the corresponding wavelet spectra (b) is displayed. The experimentally measured chirp insonating the bubble is also characterized (c,d).

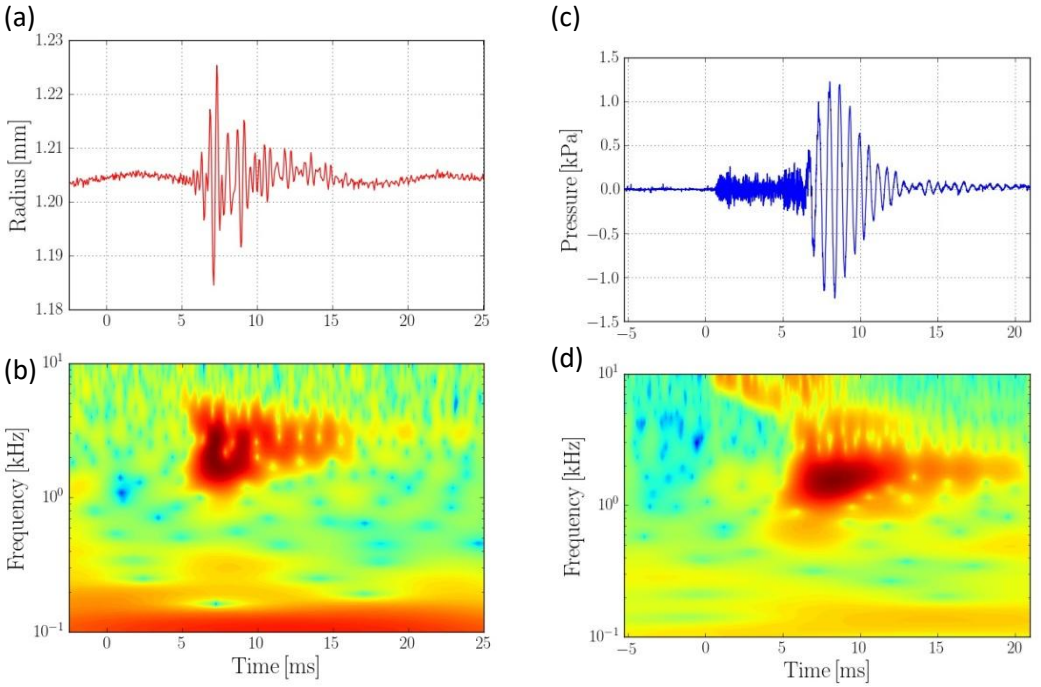

Figure 24. Results obtained for session v4. The bubble radius time evolution (a), together with the corresponding wavelet spectra (b) is displayed. The experimentally measured chirp insonating the bubble is also characterized (c,d).

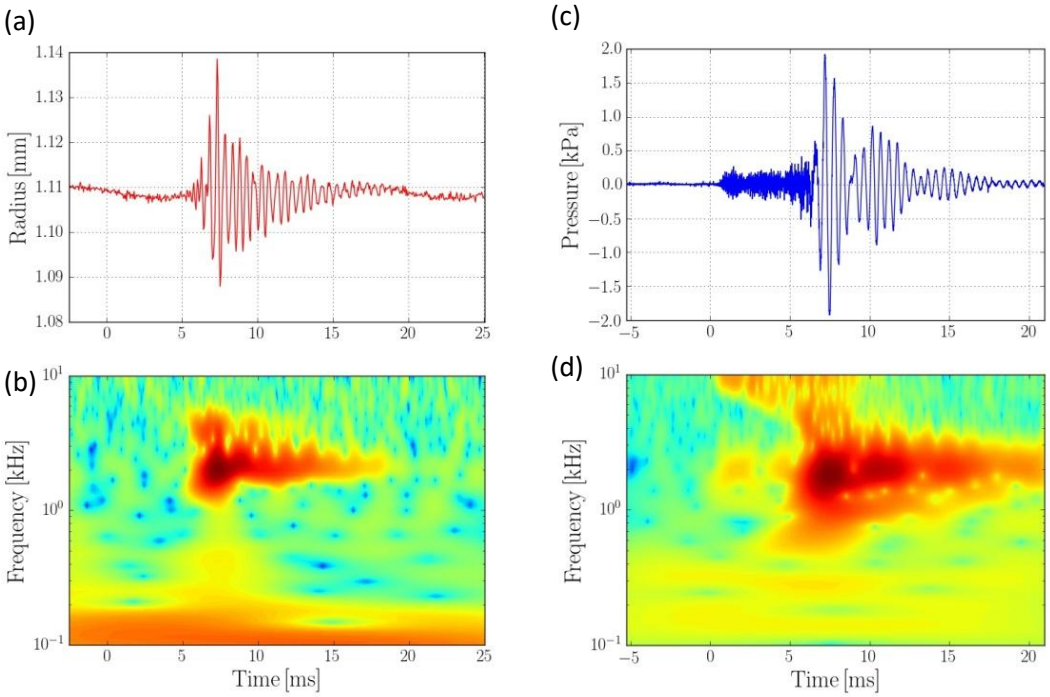

Figure 25. Results obtained for session v5. The bubble radius time evolution (a), together with the corresponding wavelet spectra (b) is displayed. The experimentally measured chirp insonating the bubble is also characterized (c,d).

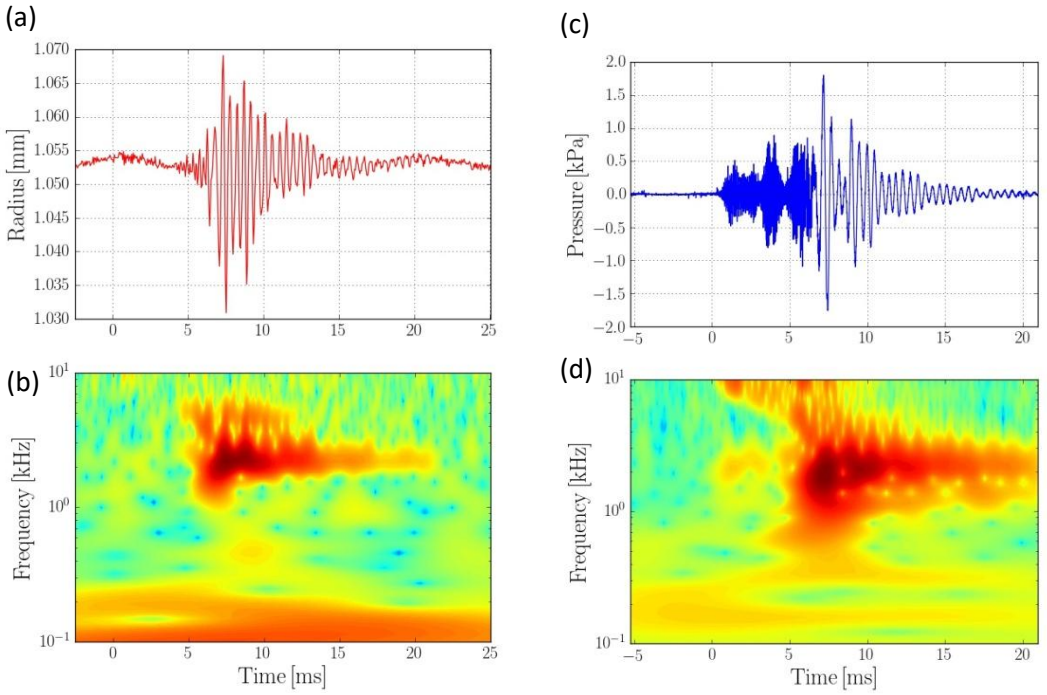

Figure 26. Results obtained for session v7. The bubble radius time evolution (a), together with the corresponding wavelet spectra (b) is displayed. The experimentally measured chirp insonating the bubble is also characterized (c,d).

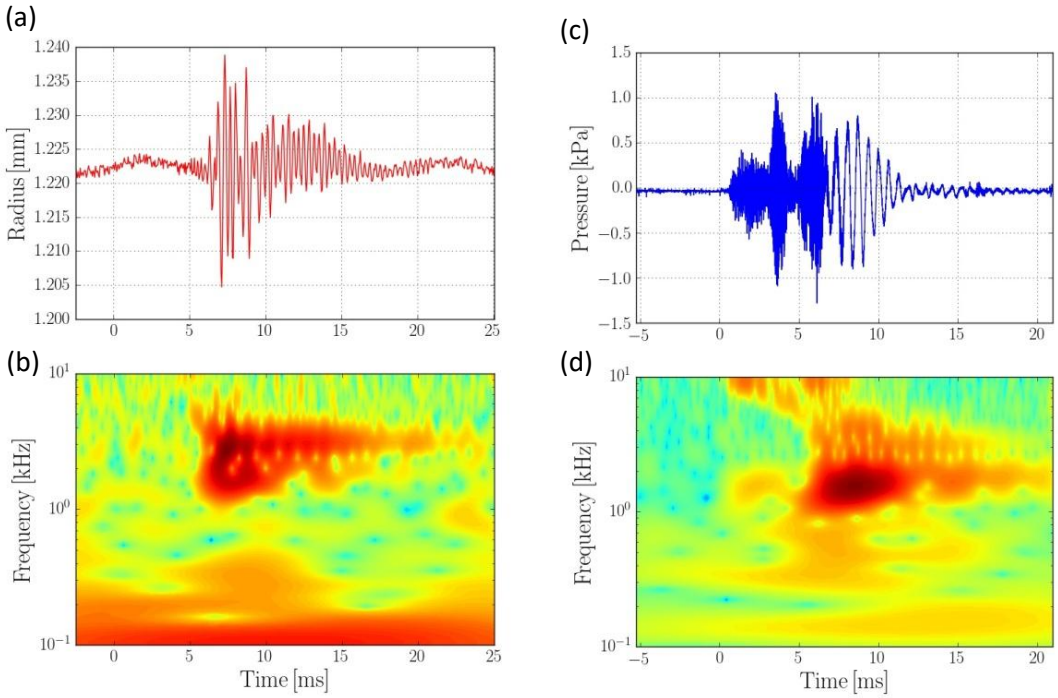

Figure 27. Results obtained for session v8. The bubble radius time evolution (a), together with the corresponding wavelet spectra (b) is displayed. The experimentally measured chirp insonating the bubble is also characterized (c,d).

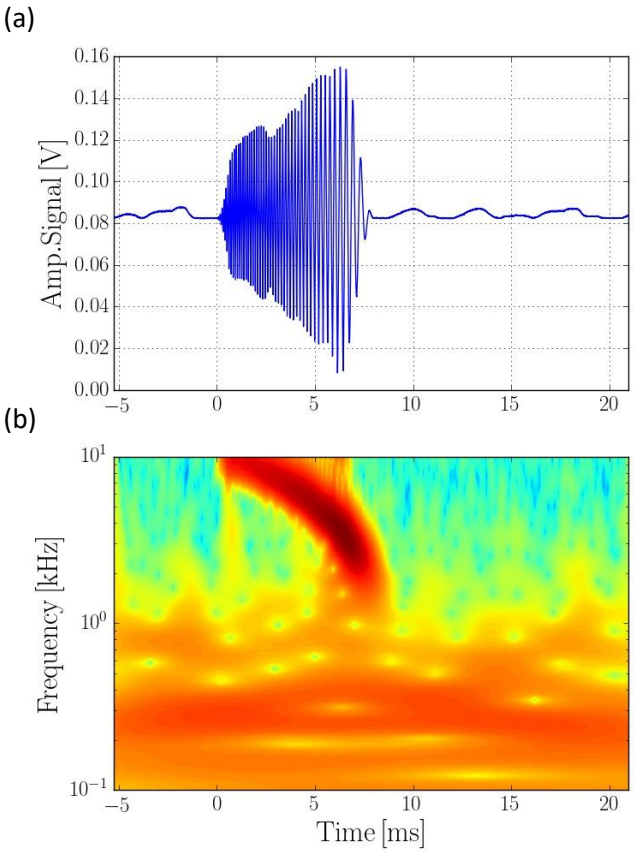

Figure 28. Electrical signal from the wave generator measured after amplification (a), and its corresponding wavelet spectra (b).

6. Regulatory Framework and Socio-economic Context

6.1. Regulatory Framework

- **Potential use of Ultrasound Contrast Agents in future applications of the technique**

As pointed out by Bettinger and Tranquart (Therapeutic Ultrasound (Advances in Experimental Medicine and Biology) Springer, 1st ed. 2016), although UCAs have proven to be mostly safe along the long time that they have been used, introducing new formulations that may incorporate different chemicals in its coating or changes in the manufacturing procedure may present a difficulty from the point of view of their approval by health authorities. This specially true in the case of UCAs that may serve as non-invasive pressure proves, since they require novel properties, as is described in the introduction of this dissertation.

- **Software licensing**

Two main software packages have been used in this project: Matlab and Python. The former is a copyrighted package whose license is covered by the university, whereas the latter is an open-source, GPL language.

The reason for using two languages with similar capabilities is that, in the group where I have developed my worked, there exists a trend to migrate all their codes to open platforms but, at the same time, it was desirable to use software tools developed by the group in the past. Since some of the algorithms developed in this project (communication with the DS345 function generator and opening video files) took as starting point existing codes, it was considered practical to extend these codes in the same language they were written.

Finally, the synchronization between the acoustic pulse (function generator), the pressure acquisition system and the high-speed camera was implemented in LabView. LabView is a graphical programming language that presents the major advantage of having available drivers to communicate with many lab equipment. The license for this software is paid for by the Department of Thermal and Fluids Engineering where I have carried out my work.

6.2. Socio-economic Context

Cardiovascular diseases are currently the number one cause of dead globally, and their early diagnosis and treatment is crucial to reduce their incidence. Among them, pulmonary arterial hypertension (PAH) has an estimated prevalence of 30 to 50 cases per million individuals [86], potentially becoming chronic and leading to death if untreated. Thus, the cost associated with the long-term treatment for this disease are considerably high.

Given the scarce physical signs and nonspecific symptoms at early stages, it is usually not detected until irreversible pathophysiologic changes have occurred, as the only means for its diagnosis at the moment is through right-side heart catheterization.

For this reason, a noninvasive technique based on UCA's for the measurement of pressure at points of difficult access in the vascular system would result into a great benefit and profit for both patients and physicians, due to the low cost and simplicity of the procedure.

Despite of the fact that the experimental approach proposed in this thesis for the study of the suitability of developing this technique has not yield conclusive results yet, we believe that the approach is the correct one and that it is just a matter of time and resources to achieve this final goal, resulting into a great benefit for the people afflicted by this disease.

- **Project Budget**

The invested in this thesis was 10 months. The project costs are described below, although most of the equipment had been already purchased for different projects by the start of this thesis.

HUMAN RESOURCES COST	Cost (€/hour)	Dedicated hours	Total cost (€)
Student	10.5[4]	700	7,350

MATERIAL COST	Cost (€)
Porcine skin gelatin (500g)	120
High-speed camera	60,000
Pressurizable chamber and piezoelectric transducer	24,000

[4] This quantity corresponds to the minimum salary perceived by a bachelor postgraduate working in a research project at Universidad Carlos III de Madrid, as an example of the usual human resources costs associated with this type of project.

Acquisition system and computer	8,500
Dynamic sensor	1,800
Static sensor	300
Waveform generator and amplifier	1,800

TOTAL PROJECT COST (€)	103,870

7. Conclusions and Future Work

Regarding the initial objectives described in this report, it can be claimed that all the **technical** objectives of this bachelor thesis have been fulfilled:

- Implementation of the experimental setup and protocol.
- Implementation of the required signal and image analysis tools.
- Determination of a suitable range of parameters to perform the experiments.
- Implementation of a simulation tool to be used as a guide for the optimisation of the experimental measurements and their interpretation.

This has been verified both with numerical simulations as well as with experiments were the bubbles were insonated with a chirp-like pressure wave and variations described by the bubble radius were accurately characterised with a sub-pixel resolution of 1.2 µm. The oscillation frequency exhibited by the bubbles was successfully detected, despite of this not being equivalent to the one corresponding to the bubble resonance frequency, but to the intrinsic one dominating the piezoelectric transducer response. As a consequence, changes with ambient pressure variations in the oscillating frequency have not been detected yet. Nevertheless, as the measured frequencies are in the same range than the expected resonance ones, we are encouraged to believe that once a proper piezoelectric transducer is put in place, we will be able to detect resonant oscillations.

Unfortunately, the substitution of the transducer with a new one with a more accurate frequency response will not be possible by the time this thesis will be defended. Nonetheless, as part of a fellowship in the Fluid Mechanics Research Group of the university, the experiments described in this thesis will be continued by the author, as the remaining objective of this thesis (the characterisation of the bubble resonance frequency changes with ambient pressure) is expected to be fulfilled once the equipment has been updated.

For this reason, as part of the planned future work, there is the replacement of the piezoelectric transducer employed for these experiments by a new one capable of operating more accurately in a wider range of frequencies, allowing for the employment of bubbles with a size closer to the ones use in real medical applications.

In addition to this, the implementation of an acoustic camera [77] is being considered, which is based on the idea of detecting the bubble radius variations by means of a pressure wave with much higher frequency than the one used to insonate the bubbles, as an alternative for the usage of a high-speed camera, constituting a fully noninvasive approach.

References

[1] R. Gramiak, P. M. Shah, and P. M. Shah, "Echocardiography of the aortic root," *Investigative radiology,* vol. 3, no. 5, pp. 356-366, 1968.

[2] A. A. Bove, M. C. Ziskin, and W. L. Mulchin, "Ultrasonic detection of in-vivo cavitation and pressure effects of high-speed injections through catheters," (in eng), *Invest Radiol,* vol. 4, no. 4, pp. 236-40, Jul-Aug 1969.

[3] F. W. Kremkau, R. Gramiak, E. L. Carstensen, P. M. Shah, and D. H. Kramer, "Ultrasonic detection of cavitation at catheter tips," (in eng), *Am J Roentgenol Radium Ther Nucl Med,* vol. 110, no. 1, pp. 177-83, Sep 1970.

[4] E. C. Unger, P. J. Lund, D. K. Shen, T. A. Fritz, D. Yellowhair, and T. E. New, "Nitrogen-filled liposomes as a vascular US contrast agent: preliminary evaluation," (in eng), *Radiology,* vol. 185, no. 2, pp. 453-6, Nov 1992.

[5] S. B. Feinstein *et al.*, "Two-dimensional contrast echocardiography. I. In vitro development and quantitative analysis of echo contrast agents," (in eng), *J Am Coll Cardiol,* vol. 3, no. 1, pp. 14-20, Jan 1984.

[6] R. Schlief and U. Deichert, "Hysterosalpingo-contrast sonography of the uterus and fallopian tubes: results of a clinical trial of a new contrast medium in 120 patients," (in eng), *Radiology,* vol. 178, no. 1, pp. 213-5, Jan 1991.

[7] F. Forsberg *et al.*, "Effect of filling gases on the backscatter from contrast microbubbles: theory and in vivo measurements," (in eng), *Ultrasound Med Biol,* vol. 25, no. 8, pp. 1203-11, Oct 1999.

[8] E. Quaia, "Contrast-specific ultrasound techniques," *La radiologia medica,* journal article vol. 112, no. 4, pp. 473-490, 2007.

[9] G. Paradossi, P. Pellegretti, and A. Trucco, *Ultrasound Contrast Agents: Targeting and Processing Methods for Theranostics*. 2010.

[10] E. Quaia, "Classification and safety of microbubbles-based contrast agents," in *Contrast Media in Ultrasonography: Basic Principles and Clinical Applications*: Springer-Verlag Berlin Heidelberg, 2005, pp. 3-14.

[11] E. Quaia, "Microbubble ultrasound contrast agents: an update," *European Radiology,* journal article vol. 17, no. 8, pp. 1995-2008, 2007.

[12] B. B. Goldberg, "Composition of contrast microbubbles: Basic chemistry of encapsulated and surfactant-coated bubbles," in *Ultrasound contrast agents: basic principles and clinical applications*, M. Dunitz, Ed., 2001, pp. 3-14.

[13] R. A. Hulst, R. A. Hulst, J. Klein, and B. Lachmann, "Gas embolism: pathophysiology and treatment," *Clinical physiology and functional imaging,* vol. 23, no. 5, pp. 237-246, 2003.

[14] B. P. Murphy, F. J. Harford, and F. S. Cramer, "Cerebral air embolism resulting from invasive medical procedures. Treatment with hyperbaric oxygen," *Annals of Surgery,* vol. 201, no. 2, pp. 242-245, 1985.

[15] J.-B. Liu, G. Wansaicheong, D. A. Merton, F. Forsberg, and B. B. Goldberg, "Contrast-enhanced Ultrasound Imaging: State of the Art," *Journal of Medical Ultrasound,* vol. 13, no. 3, pp. 109-126, 2005/01/01 2005.

[16] A. Bouakaz, N. de Jong, C. Cachard, and K. Jouini, "On the effect of lung filtering and cardiac pressure on the standard properties of ultrasound contrast agent," (in eng), *Ultrasonics,* vol. 36, no. 1-5, pp. 703-8, Feb 1998.

[17] P. Hauff *et al.*, "Delineation of experimental liver tumors in rabbits by a new ultrasound contrast agent and stimulated acoustic emission," (in eng), *Invest Radiol,* vol. 32, no. 2, pp. 94-9, Feb 1997.

[18] M. Blomley, T. Albrecht, D. Cosgrove, V. Jayaram, J. Butler-Barnes, and R. Eckersley, "Stimulated acoustic emission in liver parenchyma with Levovist," (in eng), *Lancet,* vol. 351, no. 9102, p. 568, Feb 21 1998.

[19] F. Forsberg, B. B. Goldberg, J. B. Liu, D. A. Merton, N. M. Rawool, and W. T. Shi, "Tissue-specific US contrast agent for evaluation of hepatic and splenic parenchyma," (in eng), *Radiology,* vol. 210, no. 1, pp. 125-32, Jan 1999.

[20] E. Quaia *et al.*, "Initial observations on the effect of irradiation on the liver-specific uptake of Levovist," (in eng), *Eur J Radiol,* vol. 41, no. 3, pp. 192-9, Mar 2002.

[21] G. M. Kindberg, H. Tolleshaug, N. Roos, and T. Skotland, "Hepatic clearance of Sonazoid perfluorobutane microbubbles by Kupffer cells does not reduce the ability of liver to phagocytose or degrade albumin microspheres," (in eng), *Cell Tissue Res,* vol. 312, no. 1, pp. 49-54, Apr 2003.

[22] C. J. Harvey, M. J. Blomley, R. J. Eckersley, and D. O. Cosgrove, "Developments in ultrasound contrast media," (in eng), *Eur Radiol,* vol. 11, no. 4, pp. 675-89, 2001.

[23] J. M. Correas, L. Bridal, A. Lesavre, A. Mejean, M. Claudon, and O. Helenon, "Ultrasound contrast agents: properties, principles of action, tolerance, and artifacts," (in eng), *Eur Radiol,* vol. 11, no. 8, pp. 1316-28, 2001.

[24] M. Claudon, P. F. Plouin, G. M. Baxter, T. Rohban, and D. M. Devos, "Renal arteries in patients at risk of renal arterial stenosis: multicenter evaluation of the echo-enhancer SH U 508A at color and spectral Doppler US. Levovist Renal Artery Stenosis Study Group," (in eng), *Radiology,* vol. 214, no. 3, pp. 739-46, Mar 2000.

[25] S. H. Kim *et al.*, "Value of contrast-enhanced sonography for the characterization of focal hepatic lesions in patients with diffuse liver disease: receiver operating characteristic analysis," (in eng), *AJR Am J Roentgenol,* vol. 184, no. 4, pp. 1077-84, Apr 2005.

[26] E. Quaia *et al.*, "Characterization of focal liver lesions with contrast-specific US modes and a sulfur hexafluoride-filled microbubble contrast agent: diagnostic performance and confidence," (in eng), *Radiology,* vol. 232, no. 2, pp. 420-30, Aug 2004.

[27] C. Nicolau *et al.*, "Importance of evaluating all vascular phases on contrast-enhanced sonography in the differentiation of benign from malignant focal liver lesions," (in eng), *AJR Am J Roentgenol,* vol. 186, no. 1, pp. 158-67, Jan 2006.

[28] E. Leen, P. Ceccotti, C. Kalogeropoulou, W. J. Angerson, S. J. Moug, and P. G. Horgan, "Prospective multicenter trial evaluating a novel method of characterizing focal liver lesions using contrast-enhanced sonography," (in eng), *AJR Am J Roentgenol,* vol. 186, no. 6, pp. 1551-9, Jun 2006.

[29] J. D. Berry and P. S. Sidhu, "Microbubble contrast-enhanced ultrasound in liver transplantation," (in eng), *Eur Radiol,* vol. 14 Suppl 8, pp. P96-103, Oct 2004.

[30] S. Rossi *et al.*, "Contrast-enhanced versus conventional and color Doppler sonography for the detection of thrombosis of the portal and hepatic venous systems," (in eng), *AJR Am J Roentgenol,* vol. 186, no. 3, pp. 763-73, Mar 2006.

[31] L. Tarantino *et al.*, "Diagnosis of benign and malignant portal vein thrombosis in cirrhotic patients with hepatocellular carcinoma: color Doppler US, contrast-enhanced US, and fine-needle biopsy," (in eng), *Abdom Imaging,* vol. 31, no. 5, pp. 537-44, Sep-Oct 2006.

[32] C. J. Harvey, A. K. P. Lim, M. Lynch, M. J. K. Blomley, and D. O. Cosgrove, "Applications of Ultrasound Microbubbles in the Spleen," in *Contrast Media in Ultrasonography: Basic Principles and Clinical Applications*, E. Quaia, Ed. Berlin, Heidelberg: Springer Berlin Heidelberg, 2005, pp. 205-219.

[33] O. Catalano, F. Sandomenico, I. Matarazzo, and A. Siani, "Contrast-enhanced sonography of the spleen," (in eng), *AJR Am J Roentgenol,* vol. 184, no. 4, pp. 1150-6, Apr 2005.

[34] T. K. Slabaugh, Z. Machaidze, R. Hennigar, and K. Ogan, "Monitoring radiofrequency renal lesions in real time using contrast-enhanced ultrasonography: a porcine model," (in eng), *J Endourol,* vol. 19, no. 5, pp. 579-83, Jun 2005.

[35] A. P. Miller and N. C. Nanda, "Contrast echocardiography: new agents," *Ultrasound in Medicine & Biology,* vol. 30, no. 4, pp. 425-434, 4// 2004.

[36] M. J. Stewart, "Contrast echocardiography," (in eng), *Heart,* vol. 89, no. 3, pp. 342-8, Mar 2003.

[37] P. S. Sidhu *et al.*, "Diagnostic efficacy of SonoVue, a second generation contrast agent, in the assessment of extracranial carotid or peripheral arteries using colour and spectral Doppler ultrasound: a multicentre study," (in eng), *Br J Radiol,* vol. 79, no. 937, pp. 44-51, Jan 2006.

[38] T. Holscher, W. G. Wilkening, P. D. Lyden, and R. F. Mattrey, "Transcranial ultrasound angiography (T USA): a new approach for contrast specific imaging of intracranial arteries," (in eng), *Ultrasound Med Biol,* vol. 31, no. 8, pp. 1001-6, Aug 2005.

[39] H. Leong-Poi, J. Christiansen, A. L. Klibanov, S. Kaul, and J. R. Lindner, "Noninvasive assessment of angiogenesis by ultrasound and microbubbles targeted to alpha(v)-integrins," (in eng), *Circulation,* vol. 107, no. 3, pp. 455-60, Jan 28 2003.

[40] R. J. Price and S. Kaul, "Contrast ultrasound targeted drug and gene delivery: an update on a new therapeutic modality," (in eng), *J Cardiovasc Pharmacol Ther,* vol. 7, no. 3, pp. 171-80, Jul 2002.

[41] J. P. Christiansen and J. R. Lindner, "Molecular and Cellular Imaging with Targeted Contrast Ultrasound," *Proceedings of the IEEE,* vol. 93, no. 4, pp. 809-818, 2005.

[42] K. C. Crowder *et al.*, "Augmented and selective delivery of liquid perfluorocarbon nanoparticles to melanoma cells with noncavitational ultrasound," in *IEEE Symposium on Ultrasonics, 2003*, 2003, vol. 1, pp. 532-535 Vol.1.

[43] G. Trübestein, C. Engel, F. Etzel, A. Sobbe, H. Cremer, and U. Stumpff, "Thrombolysis by Ultrasound," *Clinical Science,* vol. 51, no. s3, pp. 697s-698s, 1976.

[44] J. E. Lingeman, "Extracorporeal shock wave lithotripsy. Development, instrumentation, and current status," (in eng), *Urol Clin North Am,* vol. 24, no. 1, pp. 185-211, Feb 1997.

[45] W. W. Roberts, T. L. Hall, K. Ives, J. S. Wolf, Jr., J. B. Fowlkes, and C. A. Cain, "Pulsed cavitational ultrasound: a noninvasive technology for controlled tissue ablation (histotripsy) in the rabbit kidney," (in eng), *J Urol,* vol. 175, no. 2, pp. 734-8, Feb 2006.

[46] H. L. Liu, C. H. Fan, C. Y. Ting, and C. K. Yeh, "Combining microbubbles and ultrasound for drug delivery to brain tumors: current progress and overview," (in eng), *Theranostics,* vol. 4, no. 4, pp. 432-44, 2014.

[47] J. T. Sutton, K. J. Haworth, G. Pyne-Geithman, and C. K. Holland, "Ultrasound-mediated drug delivery for cardiovascular disease," (in eng), *Expert Opin Drug Deliv,* vol. 10, no. 5, pp. 573-92, May 2013.

[48] R. V. Shohet *et al.*, "Echocardiographic destruction of albumin microbubbles directs gene delivery to the myocardium," (in eng), *Circulation,* vol. 101, no. 22, pp. 2554-6, Jun 06 2000.

[49] W. M. Fairbank and M. O. Scully, "A new noninvasive technique for cardiac pressure measurement: resonant scattering of ultrasound from bubbles," *IEEE Transactions on Biomedical Engineering,* vol. BME-24, no. 2, pp. 107-110, 1977.

[50] M. Minnaert, "XVI. On musical air-bubbles and the sounds of running water," *The London, Edinburgh, and Dublin Philosophical Magazine and Journal of Science,* vol. 16, no. 104, pp. 235-248, 1933/08/01 1933.

[51] H. G. Flynn, "Cavitation dynamics. I. A mathematical formulation," *The Journal of the Acoustical Society of America,* vol. 57, no. 6, pp. 1379-1396, 1975.

[52] E. Quaia, *Contrast Media in Ultrasonography: Basic Principles and Clinical Applications*. Springer-Verlag Berlin Heidelberg, 2005.

[53] L. J. Rubin, "Primary pulmonary hypertension," (in eng), *N Engl J Med,* vol. 336, no. 2, pp. 111-7, Jan 09 1997.

[54] G. Simonneau *et al.*, "Updated clinical classification of pulmonary hypertension," (in eng), *J Am Coll Cardiol,* vol. 54, no. 1 Suppl, pp. S43-54, Jun 30 2009.

[55] R. Agarwal and M. Gomberg-Maitland, "Current therapeutics and practical management strategies for pulmonary arterial hypertension," (in eng), *Am Heart J,* vol. 162, no. 2, pp. 201-13, Aug 2011.

[56] D. S. O'Callaghan *et al.*, "Treatment of pulmonary arterial hypertension with targeted therapies," (in eng), *Nat Rev Cardiol,* vol. 8, no. 9, pp. 526-38, Jul 19 2011.

[57] A. L. Strauss, F. J. Roth, and H. Rieger, "Noninvasive assessment of pressure gradients across iliac artery stenoses: duplex and catheter correlative study," (in eng), *J Ultrasound Med,* vol. 12, no. 1, pp. 17-22, Jan 1993.

[58] W. T. Shi, F. Forsberg, J. S. Raichlen, and L. Needleman, "Pressure dependence of subharmonic signals from contrast microbubbles," *Ultrasound in medicine & biology,* vol. 25, no. 2, p. 275, 1999.

[59] V. G. Halldorsdottir *et al.*, "Subharmonic contrast microbubble signals for noninvasive pressure estimation under static and dynamic flow conditions," *Ultrasonic Imaging,* vol. 33, no. 3, pp. 153-164, 2011.

[60] J. R. Eisenbrey *et al.*, "Subharmonic aided pressure estimation in patients with suspected portal hypertension," in *2011 IEEE International Ultrasonics Symposium*, 2011, pp. 620-623.

[61] J. K. Dave *et al.*, "On the utility of subharmonic microbubble signals to detect portal hypertension," in *2012 IEEE International Ultrasonics Symposium*, 2012, pp. 655-658.

[62] J. K. Dave *et al.*, "Noninvasive right ventricular pressure estimation in vivo using the subharmonic emissions from ultrasound contrast agents," in *2012 IEEE International Ultrasonics Symposium*, 2012, pp. 1114-1117.

[63] F. Li *et al.*, "Ambient pressure dependence of the subharmonic signal from ultrasound contrast microbubbles," in *2012 IEEE International Ultrasonics Symposium*, 2012, pp. 663-666.

[64] K. S. Andersen, J. Jensen, Oslash, and A. Rgen, "Ambient pressure sensitivity of microbubbles investigated through a parameter study," *The Journal of the Acoustical Society of America,* vol. 126, no. 6, pp. 3350-3358, 2009.

[65] K. S. Andersen, J. Jensen, Oslash, and A. Rgen, "Impact of acoustic pressure on ambient pressure estimation using ultrasound contrast agent," *Ultrasonics,* vol. 50, no. 2, pp. 294-299, 2010.

[66] D. Adam, M. Sapunar, and E. Burla, "On the relationship between encapsulated ultrasound contrast agent and pressure," *Ultrasound in medicine & biology,* vol. 31, no. 5, pp. 673-686, 2005.

[67] Y. Ganor, D. Adam, and E. Kimmel, "Time and pressure dependence of acoustic signals radiated from microbubbles," (in eng), *Ultrasound Med Biol,* vol. 31, no. 10, pp. 1367-74, Oct 2005.

[68] A. Bouakaz, P. J. Frinking, N. de Jong, and N. Bom, "Noninvasive measurement of the hydrostatic pressure in a fluid-filled cavity based on the disappearance time of micrometer-sized free gas bubbles," *Ultrasound in medicine & biology,* vol. 25, no. 9, p. 1407, 1999.

[69] N. de Jong, F. J. ten Cate, W. B. Vletter, and J. R. Roelandt, "Quantification of transpulmonary echocontrast effects," (in eng), *Ultrasound Med Biol,* vol. 19, no. 4, pp. 279-88, 1993.

[70] M. Postema, A. Bouakaz, and N. de Jong, "Noninvasive microbubble-based pressure measurements: a simulation study," *Ultrasonics,* vol. 42, no. 1, pp. 759-762, 2004.

[71] T. G. Leighton and A. J. Walton, "An experimental study of the sound emitted from gas bubbles in a liquid," *European Journal of Physics,* vol. 8, no. 2, p. 98, 1987.

[72] B. Aldham, R. Manasseh, S. Illesinghe, K. Liffman, A. Ooi, and I. D. Šutalo, "Measurement of pressure on a surface using bubble acoustic resonances," *Measurement Science and Technology,* vol. 21, no. 2, p. 027002, 2010.

[73] S. M. v. d. Meer *et al.*, "Microbubble spectroscopy of ultrasound contrast agents," *The Journal of the Acoustical Society of America,* vol. 121, no. 1, pp. 648-656, 2007.

[74] J. Rodríguez, A. Sevilla, C. Martínez-Bazán, and J. M. Gordillo, "Generation of Microbubbles with Applications to Industry and Medicine," *Annual Review of Fluid Mechanics,* vol. 47, no. 1, pp. 405-429, 2015.

[75] E. Castro-Hernandez, W. van Hoeve, D. Lohse, and J. M. Gordillo, "Microbubble generation in a co-flow device operated in a new regime," *Lab on a Chip,* 10.1039/C0LC00731E vol. 11, no. 12, pp. 2023-2029, 2011.

[76] J. M. Solano-Altamirano, J. D. Malcolm, and S. Goldman, "Gas bubble dynamics in soft materials," *Soft Matter,* vol. 11, no. 1, pp. 202-10, Jan 07 2015.

[77] G. Renaud, J. G. Bosch, A. F. W. v. d. Steen, and N. d. Jong, "Chirp resonance spectroscopy of single lipid-coated microbubbles using an “acoustical camera”," *The Journal of the Acoustical Society of America,* vol. 132, no. 6, pp. EL470-EL475, 2012.

[78] F. Hamaguchi and K. Ando, "Linear oscillation of gas bubbles in a viscoelastic material under ultrasound irradiation," *Physics of Fluids,* vol. 27, no. 11, p. 113103, 2015.

[79] E. Stride and N. Saffari, "Investigating the significance of multiple scattering in ultrasound contrast agent particle populations," (in eng), *IEEE Trans Ultrason Ferroelectr Freq Control,* vol. 52, no. 12, pp. 2332-45, Dec 2005.

[80] L. Rayleigh, "VIII. On the pressure developed in a liquid during the collapse of a spherical cavity," *Philosophical Magazine Series 6,* vol. 34, no. 200, pp. 94-98, 1917/08/01 1917.

[81] M. Plesset, "The dynamics of cavitation bubbles.," *Journal of Applied Mechanics,* vol. 16, pp. 277-282, 1949.

[82] M. Overvelde, H. J. Vos, N. de Jong, and M. Versluis, "Ultrasound Contrast Agent Microbubble Dynamics.," in *Contrast Media in Ultrasonography: Basic Principles and Clinical Applications.*, 2005, pp. 79-97.

[83] X. Yang and C. C. Church, "A model for the dynamics of gas bubbles in soft tissue," (in eng), *J Acoust Soc Am,* vol. 118, no. 6, pp. 3595-606, Dec 2005.

[84] A. Prosperetti, "Thermal effects and damping mechanisms in the forced radial oscillations of gas bubbles in liquids," *The Journal of the Acoustical Society of America,* vol. 61, no. 1, pp. 17-27, 1977.

[85] C. Torrence and G. P. Compo, "A Practical Guide to Wavelet Analysis," *Bulletin of the American Meteorological Society,* vol. 79, no. 1, pp. 61-78, 1998.

[86] E. Bossone *et al.*, "Echocardiography in pulmonary arterial hypertension: from diagnosis to prognosis," (in eng), *J Am Soc Echocardiogr,* vol. 26, no. 1, pp. 1-14, Jan 2013.